Bioactive Materials 39 (2024) 456–478

Contents lists available at ScienceDirect

Bioactive Materials

journal homepage: www.keaipublishing.com/en/journals/bioactive-materials

Review article

An overview of magnesium-based implants in orthopaedics and a prospect of its application in spine fusion

Xuan He [a], Ye Li [b], Da Zou [a], Haiyue Zu [c], Weishi Li [a,*], Yufeng Zheng [d,**]

[a] Department of Orthopaedics, Peking University Third Hospital, No.49 North Huayuan Road, Haidian, Beijing, PR China
[b] Department of Rehabilitation Science, The Hong Kong Polytechnic University, Hong Kong SAR, PR China
[c] Department of Orthopaedics, The First Affiliated Hospital of Suchow University, PR China
[d] Department of Materials Science and Engineering, College of Engineering, Peking University, Comprehensive Scientific Research Building, Beijing, PR China

ARTICLE INFO

Keywords:
Magnesium
Magnesium alloys
Magnesium surface modification
Magnesium implants
Spine fusion

ABSTRACT

Due to matching biomechanical properties and significant biological activity, Mg-based implants present great potential in orthopedic applications. In recent years, the biocompatibility and therapeutic effect of magnesium-based implants have been widely investigated in trauma repair. In contrast, the R&D work of Mg-based implants in spinal fusion is still limited. This review firstly introduced the general background for Mg-based implants. Secondly, the mechanical properties and degradation behaviors of Mg and its traditional and novel alloys were reviewed. Then, different surface modification techniques of Mg-based implants were described. Thirdly, this review comprehensively summarized the biological pathways of Mg degradation to promote bone formation in neuro-musculoskeletal circuit, angiogenesis with H-type vessel formation, osteogenesis with osteoblasts activation and chondrocyte ossification as an integrated system. Fourthly, this review followed the translation process of Mg-based implants via updating the preclinical studies in fracture fixation, sports trauma repair and reconstruction, and bone distraction for large bone defect. Furthermore, the pilot clinical studies were involved to demonstrate the reliable clinical safety and satisfactory bioactive effects of Mg-based implants in bone formation. Finally, this review introduced the background of spine fusion surgeryand the challenges of biological matching cage development. At last, this review prospected the translation potential of a hybrid Mg-PEEK spine fusion cage design.

1. Background of Mg-based implants R&D

Traditional orthopedic fixation equipment and prostheses are generally made of hard materials such as stainless steel, Ti or its alloys, and Co-Cr alloys. These materials presented good biocompatibility, corrosion resistance, and mechanical strength [1]. However, the typical limitations of these materials listed below may directly or indirectly jeopardize the healing outcome: firstly, during the remodeling stage, the stress shielding effect of hard metal can weaken the mechanical stimulation of the bone tissue around the implant, thereby delaying the healing process; Secondly, if nonabsorbable implants are not timely removed, it may lead to related complications, such as loosening or breakage of the implant, local pain, or infection around the implant [2,3]. Lovald et al. reported that 751 in 7391 patients removed the internal fixation hardware because mentioned complications, which is over 10 %. Among 751 patients, implants mechanical complication took 16.2 % [4]; Thirdly, patients may suffer from unpleasant feelings, risk of reoperation, and iatrogenic trauma when removing these implants [5]; Fourthly, implants retained in the body and radiological artifacts brought by implants may interfere with other treatments or surgical procedures [6]. Although biodegradable polymers can effectively compensate for the shortcomings of hard metal implants listed above [7,8], there are some disadvantages for these materials. However, the mechanical properties of polymers are relatively low. Polylactide (PLA) is mostly used polymer material in implants. Its elastic modulus and tensile strength of polylactide is 3 GPa and 50–70 MPa respectively [9].

Peer review under responsibility of KeAi Communications Co., Ltd.
* Corresponding author. Department of Orthopaedics, Peking University Third Hospital, No.49 North Huayuan Road, Haidian District, 100191, Beijing, PR China.
** Corresponding author. Department of Materials Science and Engineering, College of Engineering, Peking University, Comprehensive Scientific Research Building, Peking University, Beijing, 100871, PR China.
E-mail addresses: puh3liweishi@163.com (W. Li), yfzheng@pku.edu.cn (Y. Zheng).

https://doi.org/10.1016/j.bioactmat.2024.04.026
Received 29 December 2023; Received in revised form 22 April 2024; Accepted 22 April 2024

In addition, accumulated acidic products during polymer degradation can amplify local inflammation levels and accelerate bone resorption [10]. Because of these limitations, polymers presented lower osteogenic potential than Ti metals [11]. Summarizing the advantages and disadvantages of hard metals and polymers, implant materials for orthopedic applications should achieve moderate biomechanical properties (high strength for durable mechanical support and low Young's modulus that close to bone), safe biocompatibility (low cytotoxicity, low concentration level in circular system, low organ retention, and no ectopic ossification), and effective biological activity (osteogenesis and angiogenesis). Considering of these properties, Mg metal can be identified as a promising material, which will be comprehensively elucidated in this review.

Mg is under the name of its place of origin in history, Magnesia, Greece. In Chinese character, the left part means metal, and the right part means beautiful. In 1808, a British chemist, Sir Humphrey Davy

Table 1
Mechanical properties of Mg-based alloys.

Alloy composition	Processing condition	Yield strength MPa	Ultimate strength MPa	Elongation %	Elastic modulus GPa	Ref.
Cortical bone	/	104–121	110–130	0.7–3	3–20	[19]
Ti and its alloys	/	758–1117	/	/	110–117	[20]
High purity Mg	/	65–100	90–190	2–10	41–45	[21]
Mg-0.5Zn	extruded	T62C49	T145C237	T17.2C17.9	/	[22]
Mg–1Zn	extruded	T91C64	T169C295	T18.7C20.9	/	
Mg-1.5Zn	extruded	T101C65	T190C305	T17.2C18.5	/	
Mg–2Zn	extruded	T111C74	T198C315	T15.7C17.8	/	
Mg–1Zn–1Ca	Casting	T45	T125	T5.7	T2.13	[23]
Mg–2Zn–1Ca	Casting	T52	T143	T7.3	T2.38	
Mg–3Zn–1Ca	Casting	T57	T160	T8.3	T2.92	
Mg–4Zn–1Ca	Casting	T63	T182	T9.1	T4.42	
Mg–5Zn–1Ca	Casting	T65	T173	T8.2	T6.15	
Mg–6Zn–1Ca	Casting	T67	T145	T4.5	T9.21	
Mg-1.5Zn-0.29Ba	Rolled	T87-137	187–224	T20-22	/	[24]
Mg–Zn–Y-Nd	Casting/Extruded	T105-185	T209-303	T10.6–30.2	/	[25]
Mg–Zn–2Y	Extruded	T~170	T~290	T~28	/	[26]
Mg–Zn-xNd/Y-0.5Zr	Casting	T~80-110	T~110-215	T~5-20	/	[27]
Mg-1.6Zn-0.5Gd	Extruded	T~117	T~213	T~30	/	[28]
Mg–2Zn-0.5Gd	Extruded	T~220	T~280	T~13	/	[29]
Mg–2Zn-1Gd	Extruded	T~280	T~340	T~24	/	
Mg–2Zn-1.5Gd	Extruded	T~260	T~290	T~18	/	
Mg–2Zn-2Gd	Extruded	T~220	T~270	T~13	/	
Mg–4Zn-0.1Ce-0.3Ca	Rolled	T109-119	T231-240	T17.3–18.3	/	[30]
Mg-0.5Ca	Casting	C70.1	C166.2	C14.5	C15	[31]
Mg–1Ca	Casting	T39C72	T105C179.5	T4.1C11.5	T.3.16C16.2	[23,31]
Mg–2Ca	Casting	C77.2	C184.6	C11.2	C16.7	[31]
Mg–5Ca	Casting	C94.1	C188.4	C9.4	C18	
Mg–10Ca	Casting	C109.4	C190	C9.2	C21.7	
Mg–15Ca	Casting	C172.3	C208.1	C3.2	C26.8	
Mg–20Ca	Casting	C234.9	C291.3	C1.7	C34.8	
Mg-0.5Ca-0.5Sr	Casting	C274.3	/	/	/	[32]
Mg–1Ca-0.5Sr	Casting	C274.2	/	/	/	
Mg–1Ca–1Sr	Casting	C215.4	/	/	/	
Mg–1Zr-0.5Sr-0.5Ho	Extruded	T192.7C120.3	T239.2C388.7	T8.1C17.7	T45.4	[33]
Mg–1Zr-0.5Sr-1.5Ho	Extruded	T164.7C125.8	T225.5C347.9	T20.7C25.6	T45.2	
Mg–1Zr-0.5Sr-4Ho	Extruded	T174.1171.6	T231.1C423.4	T24.3C33.4	T47.5	
Mg–1Sr	Rolled	T~125	T~165	T~6	/	[34]
Mg–2Sr	Rolled	T~150	T213.3	T3.2	/	
Mg–3Sr	Rolled	T~115	T~165	T~3.25	/	
Mg–4Sr	Rolled	T~85	T~110	T~2.75	/	
Mg–3Sr-0.6Y	Extruded	T~150	T~450	T-4.8	/	[35]
Mg–1Y	Rolled	T~47	T~137	T~19		[36]
Mg–1Y-0.6Ca-0.4Zr	Casting	T~60 C–75	T~125 C–290	T~3 C–30	T~60	[37]
Mg–4Y-0.6Ca-0.4Zr	Casting	T~80 C–100	T~150 C–310	T~5.5 C–22	T~50	
Mg–4Y–1Mn	Casting	T~60-150	T~75-175	/	/	[38]
Mg–7Y-0.2Zn	Rolled	T310-495	T442-541	T1.9–4.6	/	[39]
Mg–8Y-0.5Zn	Extruded	T149	T246	T18.1	/	
Mg-0.16Nd	Extruded	T~60	T~330	T~20		[40]
Mg-Nd-Zn-Zr	Extruded	T90-333	T194-334	T7.9–25.9	/	[41]
Mg-0.2Ce	Rolled/Forged	T~90–110/60-64	T~170–250/160-200	T~17/38	/	[42,43]
Mg–Ce–4Zn–1Mn	Casting	T~40-90	T~40–90 T–40-150	/	/	[38]
Mg–1Mn-1Nd	Extruded	T~140	T~250	T~28	/	[44]
Mg–3Tb	Rolled	T~90	T~170	T~17	/	[45]
Mg-3Ho	Rolled	T~90	T~158	T~18	/	
Mg–3Er	Rolled	T~50	T~144	T~22	/	
Mg–3Al–1Zn	Extruded/Rolled	T165/122-175	T245/228-272	T10/14-24	/	[46–48]
Mg–3Al-0.3Mn	Extruded/Rolled	T170/134-144	T240/266-272	T12/23.8–24.9	/	[46,49]
Mg–3Al-0.4Mn	Rolled	T153-166	T255-259	T26.6–27.7	/	[50]
Mg–6Al–1Zn	Rolled	T145-152	T286-291	T23.8–25.6	/	[49]
Mg–3Al–1Zn-0.5Mn	Rolled	T157-191	T241-304	T21-25	/	[51]
Mg–17Al–7Cu–3Zn-xGd	Casting	T271-302	T402-442	T7.6–8.2	/	[52]
Mg–9Li–1Zn	Extruded	T~160	T~180	T~44.5	/	[53]
Mg–9Li–3Al–1Zn-0.2Mn	Extruded	T~110	T~165	T~45	/	

T: tensile; C: compressive; ~: precisely value was not shown in references.

identified this metal as Mg. The atom weight of Mg is 12 and molar mass is 24 g/mol. The crystal structure of pure Mg is Hexagonal Closest Packed. Mg is the fourth most abundant mineral element in the human body, fully involved in cell signaling, metabolism, and the formation of bones and soft tissues [12]. In addition, Mg^{2+} also participate in the biological functions of hundreds of enzymes [13]. Considering the mechanical strength of Mg is close to bone tissue, Payr proposed that Mg could be processed as nail or plate to fix fracture. Lambotte firstly implanted Mg fixation in patient in 1906. Unfortunately, due to the fracture of the implant during degradation and the accumulation of a large amount of hydrogen gas at the fracture site, the early stage attempts at Mg metal implants in the field of orthopedics were unsuccessful. These failures attenuated Mg implants application for decades [14]. From 1970s, the translation potential of Mg-based implants became promising with the development of Mg purification and alloy casting techniques [15], new processing techniques [16], and surface modification techniques [17,18]. This review starts with the mechanical properties, degradation properties, biocompatibility, and surface modification techniques of Mg and its alloys. Then, the biological mechanisms of Mg degradation products are demonstrated. Furthermore, the pre-clinical and clinical studies about Mg implants in orthopaedics application are summarized. Finally, the development of spine fusion cage is reviewed. The translation potential of Mg-based biological matching cage is discussed and prospected.

2. Mechanical properties of Mg-based metal

As shown in Table 1, the Young's modulus of bone ranges from 3 to 20 GPa. While that of Ti and its alloys is between 110 and 117 GPa, and of Mg is between 41 and 45 GPa. The yield strength of bone ranges from 104 to 121 MPa. While that of Ti and its alloys is between 758 and 1117 MPa, and of Mg is between 65 and 100 MPa. Compared with Ti and its alloys, both Young's modulus and yield strength of Mg are close to bone [19–21,54], which can significantly reduce the stress-shielding effect of implant interface load on bone [55]. In an alloy system, different elemental addition can affect the mechanical strength of Mg alloys

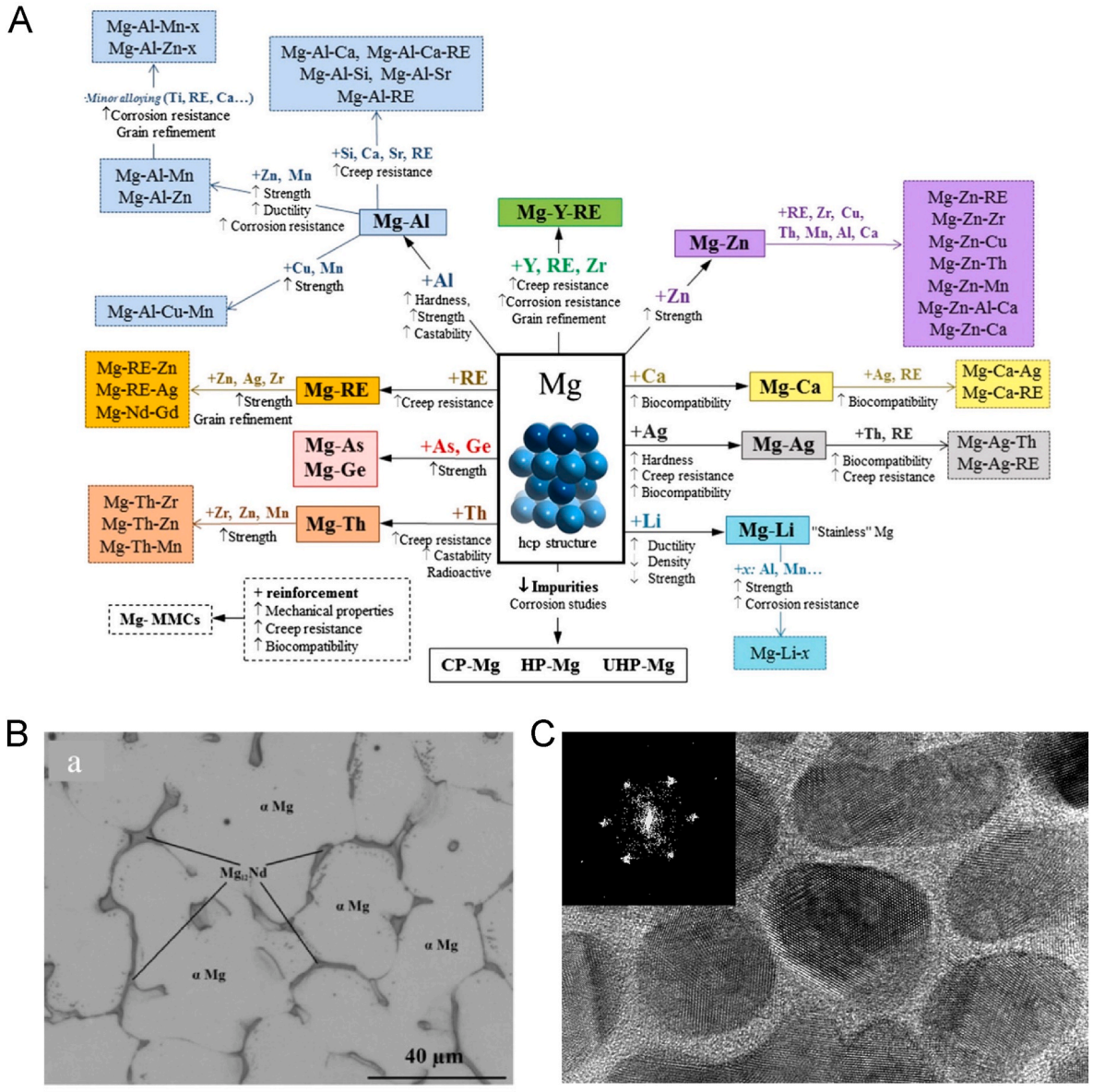

Fig. 1. A. Alloying elements additions affect Mg mechanical properties and degradation behavior, Esmaily et al. [58], copyright 2017, ELSEVIER, Creative Commons Attribution License; B. Microstructure of JDBM alloy, Zhang et al. [59], copyright 2012, ELSEVIER; C. Microstructure of Mg-based SNDP-CG alloy, Wu et al. [17], copyright 2017, Springer Nature.

(Fig. 1A). In Mg–Zn binary alloys, when the proportion of Zn element is 0.5 %, 1 %, 1.5 %, and 2 %, the corresponding compressive strength is 62 MPa, 91 MPa, 101 MPa, and 111 MPa, while the tensile strength is 145 MPa, 169 MPa, 190 MPa, and 198 MPa, respectively [22]. The compressive strength of Mg–Ca binary alloys increased with the increasing Ca weight proportion [31]. This positive correlation between mechanical strength and element weight proportion of binary alloy elements was not observed in Mg–Sr alloys [56]. The yield tensile strength of Mg-RE binary alloys such as Y, Er and Nd were around 47 MPa, 50 MPa, and 60 MPa respectively [36,40,45]. Compared to these alloys, the yield tensile strength of Mg rare earth binary alloys such as Tb, Ho, and Ce were higher which were around 90 MPa [42,43,45].

Mg tertiary alloys are more complex. In Mg–Zn tertiary alloys, excessive Zn content caused a decrease in strength [23]. The high proportion of Zn induced more second phase precipitation which could weaken the mechanical strength (4 w%) and corrosion resistance (2 w %). In addition, Mg–Zn-RE alloys involved Y, Nd, Ce, Ba and Gd elements could present higher yield strength than traditional Mg–Zn–Ca alloys [24–30]. Mg–Zn–Y-Nd (JDBM) alloy and could present 185 MPa in yield strength, 303 MPa in ultimate strength, and 30 % elongation rate [25] (Fig. 1B). Miao et al. developed a Mg–Zn-Gd alloy that behaved 316 MPa in yield strength, 354 MPa in ultimate strength, and 24 % elongation rate [29]. Mixing with 0.5 w% Sr, only 0.5 or 1 w% Ca involved tertiary alloy could reach the compressive strength level of 20 w% Ca involved binary alloy [32]. In traditional points, Al played a crucial role in Alzheimer's disease progression, whereas recent findings weakened the correlation between Al exposure and morbidity of Alzheimer's disease [57]. Therefore, Mg–Al tertiary alloys also presented promising translational potential since their good mechanical properties [46–50]. Among Mg rare earth elements based tertiary alloys [33,35,37–39,41], Mg7Y0.2Zn presented 495 MPa in yield strength and 541 MPa in ultimate strength [39]. Besides, Mg–Mn tertiary alloy [44] and Mg–Li tertiary alloys [53] also showed good balance between strength and elongation rate. Nowadays, Mg high entropy alloys within four or even more elements are well developed and researched. The high elongation rate of these high entropy alloys might be potentially applied as the implants with complex structures [51–53]. Wu et al. fabricated a supra-nanometre-sized dual-phase glass-crystal (SNDP-CG) Mg based material (Fig. 1C). The average composition of SNDP-CG is $Mg_{49}Cu_{42}Y_9$. This magnesium-based SNDP-GC presented an ultimate stress of 3.3 GPa and strain limit of 4.5 %. More important, its experimental elastic strain limit almost approaches the theoretical limit for strength [17].

3. Degradation and biocompatibility of Mg and its alloy

3.1. Degradation mode and factors that determine degradation speed

The general degradation process among Mg and its alloys is similar. Reacting with water, the $Mg(OH)_2$ and hydrogen are produced. Mg $(OH)_2$ furtherly reacts with body fluids, Mg^{2+} and $Ca_3(PO_4)_2$ (Fig. 2A). The degradation speed of Mg and its alloys was decided by multiple factors [60]. Pogorielov et al. summarized as these factors as alloying factors (type of materials, alloying elements, method of materials casting, grain size and metal purity), *in vitro* factors (solution pH, static/dynamic, solution temperature, degradation media, and degradation method), and *in vivo* factors (tissue pH, Cl^- level, vascularization of peri-implants zone, type of animal, and place of implantation) [61] (Fig. 2B). The purity of Mg significantly affected the corrosion rate. Within the impurity elements such as Ni, Fe and Cu, the degradation speed was about 50 times faster than the high purity Mg [66–68]. Henderson et al. reported that the degradation rate of Mg alloy implants was faster than that of pure Mg implants, which may be due to the electrochemical reaction between alloy elements accelerating the degradation process [69]. However, the degradation of Mg alloys is more complicated. Different alloying addition can accelerate or slow down the corrosion rate [58] (Fig. 1A). Makkar et al. reported that Ca should not exceed 1w% in alloys, or it could induce textures. They found the degradation speed of Mg5Ca was significantly faster than Mg0.5Ca. Relatively low Zn content could improve corrosion resistance [70]. When Zn exceeds 5 w% in alloy system, the corrosion resistance and mechanical properties can be weakened by second phase precipitation [71,72]. Al in alloys present better grain refinement, which is important to control the corrosion rate. Although the solubility of Al in alloys can reach 12.7 w%, the biocompatibility of high dosage Al is concerned [73]. Mn can improve corrosion resistance mostly in ternary alloys by converting the impurities into intermetallic compounds [74]. Within Zr, the alloys show good corrosion resistance against salt solutions, acids, and alkalis [75,76]. Sayari et al. reported that Zr addition developed a bimodal microstructure and decreased the grain size [77]. Sr addition contributes grain refinement [78]. Jiang et al. reported that Mg1Sr and Mg2Sr showed lowest corrosion rate than other Mg–Sr alloys, that indicated that Sr addition should not over 2 w% [79]. Li addition prominently activates the prismatic slips and enhance alloying microstructure [80,81]. Considering its corrosion resistance property, Mg–Li alloys were entitled as "stainless Mg" [58]. Except for mechanical properties, rare earth elements additions also benefit degradation behavior with the stable degradation product layer [82]. Azzeddine et al. reported corrosion resistance of Dy, Gd, Ce, Nd, and La addition. Mg–La presented fastest corrosion rate because $Mg_{12}La$ phase triggered pitting corrosion, while Dy_2O_3 formation inhibits pitting corrosion on Mg–Dy alloy [83].

Hank's solution, simulated body fluid (SBF), Earle's balanced salt solution (EBSS) and minimum essential medium (MEM) are mostly used as *in vitro* degradation test media. Hank's solution and SBF content similar ions concentration to blood plasma [84]. Besides to ions, MEM also contains nutrients such as glucose, amino acid and vitamins, which can affect the degradation process [85]. Some studies reported the corrosion rate of pure Mg in Hank's solution, SBF, and EBSS was 2.05 mm $year^{-1}$, 1.39 mm $year^{-1}$, and 0.39 mm $year^{-1}$ [86–88]. High temperature environment accelerates the degradation process of Mg. Pure Mg presents 150 % and 300 % faster degradation speed at 40 °C than the speed at 37 °C and 20 °C [89]. Buffering system is important to keep the pH value at a relatively stable level to process the degradation continually [86,90]. Although $NaHCO_3/CO_2$ system can effectively maintain the pH value, the process is complicated. He et al. observed that at the beginning of degradation, the chemical reaction was intense, the pH value significantly increased, and a large amount of hydrogen gas overflowed from the metal surface [91]. After 24 h of *in vitro* degradation, the pH value began to remain stable, as the degradation products $Mg(OH)_2$, $MgCO_3$, and $Mg_3(PO_4)_2$ formed a passivation layer to temporarily slow down further degradation [62] (Fig. 2C). At this stage, it is noticed that the mass of Mg after degradation is heavier because the molecular weight of the mixture that formed the passivation layer is higher than that of Mg. As the degradation time extended, the passivation layer continued to be activated and eroded through the buffer system, and the metal structure began to break down with a decrease in weight and volume [92,93]. Since CO_2 in the air could neutralize the alkaline environment generated by degradation to a certain extent, the pH value was usually maintained at a relatively stable level during the degradation process [94–96]. To mimic the *in vivo* environment, a dynamic test that removing the passivation layers may keep degradation process more smoothly [97]. In addition, degradation method also can affect corrosion rate. As mentioned, mass loss method can mimic *in vivo* environment, but it can be retard or stopped by the degradation products and pH value [98]. On the contrary, electrochemical test is directly and reproducible, but it presents faster corrosion rate than the nature degradation process [99]. This method fails to mimic the *in vivo* degradation environment; therefore, it is not suitable as the method for implantable material.

Compared to *in vitro* degradation, the corrosion rate *in vivo* varies greatly depending on the implantation environment [100]. Unlike subcutaneous implantation of Mg alone, exposing Mg to synovial fluid,

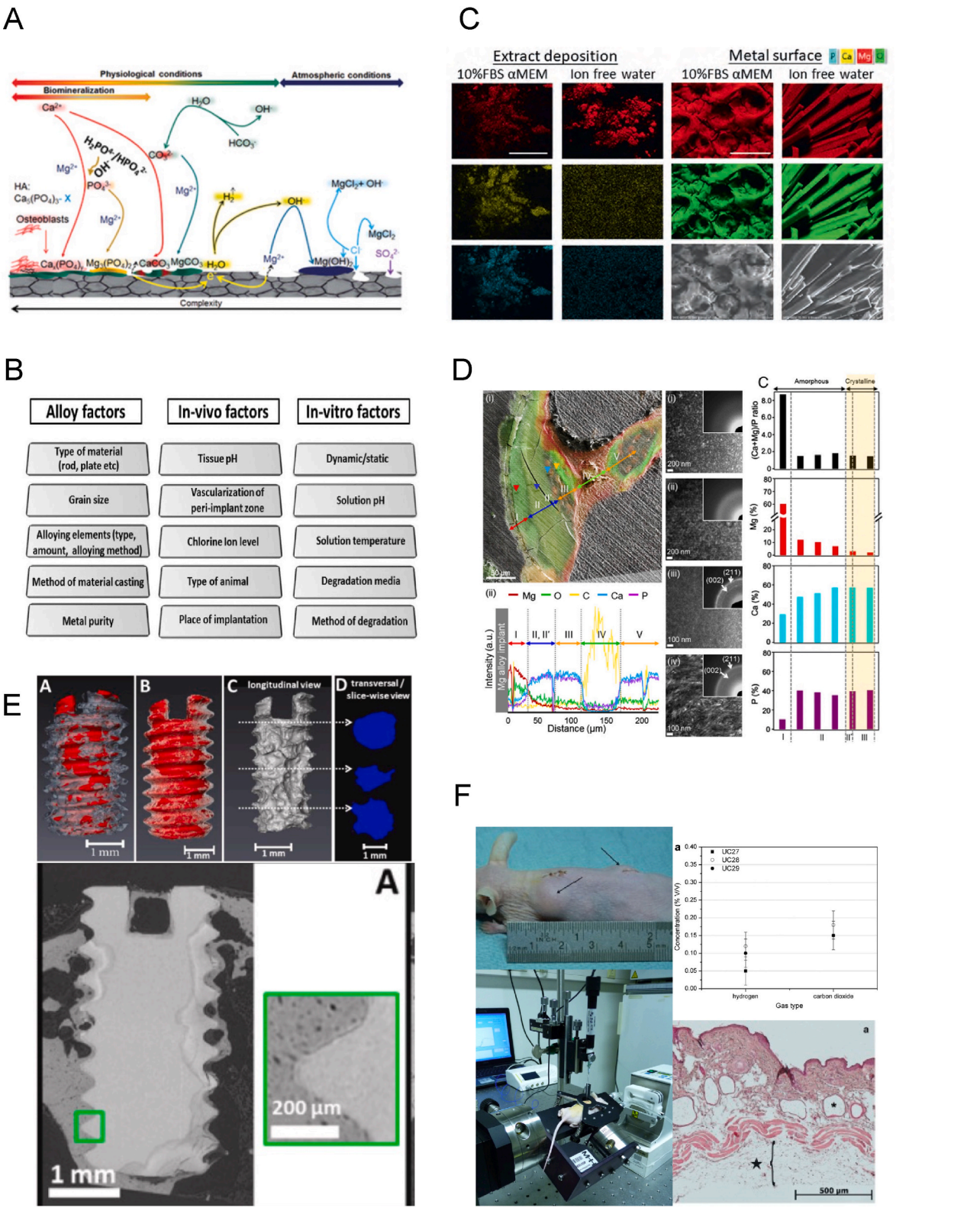

Fig. 2. A. The degradation process of Mg, Gonzalez et al. [60], copyright 2018, Ke Ai, Creative Commons Attribution License; B. Factors affect Mg degradation rate, Pogorielov et al. [61], copyright 2017, AK journals, Creative Commons Attribution License; C. Mg *in vitro* degradation products analysis, He et al. [62], copyright 2024, Ke Ai, Creative Commons Attribution License; D. Mg *in vivo* degradation products analysis, Lee et al. [63], copyright 2016, PNAS, open access; E. Mg implants *in vivo* corrosion evaluation by using a synchrotron-radiation micro CT (SRμCT), Krüger et al. [64], copyright 2022, Ke Ai, Creative Commons Attribution License; F. Hydrogen concentration in tissue cavities after Mg implantation, top left: subcutaneous gas accumulation, top right: hydrogen concentration in cavities, bottom left: amperometric hydrogen sensor and mass spectrometric measurements, bottom right: subcutaneous gas cavities, H&E staining, Kuhlmann et al. [65], copyright 2013, ELSEVIER.

blood, bone marrow, and inflammatory areas could significantly accelerate the corrosion rate [61,86]. Unlike the *in vitro* degradation mode, calcium phosphate salts could gradually replace Mg in the coating during the *in vivo* degradation process [63,101,102] (Fig. 2D). Implanting the same material in different animals or human causes different corrosion rate since the diversity of blood flow speed and water contains can accelerate degradation products clearance [99]. Compared with *in vitro* and *in vivo* degradation environment, concentration of Mg, Na, K, Ca, and pH value are similar, except concentration of Cl^-. During the degradation process, chloride are able to transform $Mg(OH)_2$ into $MgCl_2$, which is a key step to accelerate the degradation speed [103,104]. Although the pH value and temperature in musculoskeletal system is relatively stable, they may be affected by local inflammation or foreign body reaction, thus accelerating or retarding corrosion rate [105]. In addition, it is more difficult to evaluate *in vivo* degradation precisely compared to *in vitro* degradation. On one site, cleaning the tissue surround the metal may cause extra mass loss. On the other, it is hardly to identify Mg from bone tissue when using micro-CT to evaluate volume loss [106]. To solve this difficult problem, Sefa et al. and Krüger et al. applied high resolution synchrotron micro-CT (SRμCT) to evaluate Mg-based implants *in vivo* degradation [64,107]. With this technique, the boundary between Mg-based implants and bone could be observed distinctively after three dimensional and longitudinal reconstruction (Fig. 2E). Directly assessing implanted materials *in vivo* degradation can accelerate medical translational process.

3.2. Biocompatibility of degradation products

At present, the metal extraction solution is prepared following ISO10993 and GBT16886 standards [108]. For the development of medical implants, due to the crucial role of the material-tissue interface in the degradation process, the use of surface area volume ratio as the main parameter is relatively reasonable compare to weight. Some studies reported that the safe dose range of the Mg^{2+} was between 5 mmol/L and 10 mmol/L [109–111], which reflect the tolerance range in the skeletal muscle system to Mg^{2+}. Neuron cells could tolerate 30 mmol/L of Mg^{2+}, which might be due to the large number of ion channels of nerve system that could dynamically balance the intracellular and extracellular ion concentration [112]. Vascular endothelial cells also presented a high survival rate when the Mg^{2+} concentration was lower than 20 mmol/L [113]. There are two major potential factors that Mg^{2+} jeopardizes cells: 1. Magnesium ions can disturb calcium ions flowing which play crucial role in cell signaling. 2. Na^+ is the major positive ions in extracellular environment with the concentration from 135 to 145 mmol/L. Under natural condition, the concentration of Mg^{2+} is less than 1 mmol/L, which hardly elevate the extracellular positive ion concentration. A high concentration of Mg^{2+}, 10 mmol/L for instance, can significantly elevate the positive concentration which also identified as crystal osmotic pressure. A high osmotic pressure can lead cellular dehydration. The alkaline environment generated by degradation was usually safe for cells, as CO_2 in the incubator could significantly inhibit the pH value from rising and maintain it around 8 [29]. Unlike *in vitro* environments, *in vivo* systems could effectively remove degradation products. Wang et al. modified the cytotoxicity testing standards for this difference by diluting the extract 6 to 10 times for cytotoxicity testing to simulate the actual concentration in the body [114]. As for the biocompatibility of alloying elements addition, most of these elements play important roles in physiological functions. The low content in alloys of these elements hardly reaches the toxic level. Zhang et al. reported Mg6Zn implantation was harmless to major organs [115]. Jiang et al. reported a low cytotoxicity of Sr when the content below 2 w%. Mehjabeen et al. and Kim et al. confirmed the biocompatibility of Zr *in vitro* [116,117]. Al was suspected as one of pathogenic factors of brain diseases, especially Alzheimer's disease [118]. Recent study attributed the genetic factor as the major reason of Alzheimer's disease, instead of Al intaking [57]. But still, the Al addition contents should be controlled. Most of rare earth elements alloying systems presented good biocompatibility since the earth elements contents are quite low. But the potential damages and toxic effects should be highlighted when designing these alloys. Overdose Y can accumulate in liver and gallbladder, and it can elevate eosinocytes level [119]. Overdose Ce can damage liver, kidney and central neuro system [120]. Gd compound is used as the contrast media for MRI, which can indirectly show the biological safety of Gd. Although Gd also accumulate in bone and brain, when the Gd content below 1 w%, the alloys present good compatibility [121,122]. Compared with Y, Dy and Nd are more recommended for biological application since the better biocompatibility [75].

3.3. Hydrogen emission

As mentioned above, accumulating a large amount of hydrogen gas is one of the complex problems to be solved during the medical translation of Mg-based implants. During the degradation process, the yield of hydrogen gas depends on the total weight of degradable Mg, the degradation rate, and the implantation location [123]. Although some studies showed that hydrogen could promote bone formation, weaken the activity of osteoclasts [54–56] and regulate oxidative stress responses [124,125], due to the high mortality rate of air embolism, it was still necessary to strictly control hydrogen accumulation during trauma repair [123,126,127]. Currently, controlling the degradation rate of Mg to balance gas formation and absorption could solve this problem to some extent [128]. According to the chemical degradation formular, the hydrogen volume is directly related to the corrosion rate. Therefore, the key point of hydrogen emission adjustment is a controllable corrosion process. The details of managements to control corrosion are introduced in section 3.1 and section 4. While these theories and managements are based on an assumed consensus that the observed gas emission and accumulation is hydrogen. Using an amperometric hydrogen sensor and mass spectrometric measurements, Kuhlmann et al. reported a very low hydrogen concentration even shortly after gas cavities formation [65] (Fig. 2F). This interesting finding may weaken the concerns about hydrogen accumulation induced. by Mg degradation. However, it also brought new questions to investigate and answer. Firstly, if the hydrogen is swiftly exchanged by soft tissue, why the gas cavities cannot collapse? Secondly, what is the gas type to keep the gas cavities expansion? If this gas exchanges hydrogen from cavities, it is still meaningful to modulate gas accumulation by controlling Mg corrosion rate.

4. Mg and its alloy surface coating modifications

Although the degradation properties endowed the clinical translational potential of Mg implants, the high corrosion rate was also a prominent limitation and challenge in this process. The mechanical strength of Mg-based implants rapidly dropped after implantation, which induced implant fracture at the early healing stage, thus leading to almost inevitable fracture healing failure. Along this degradation process, the products involving high concentrations of Mg^{2+}, hydrogen accumulation, and an alkaline environment also jeopardized patients' health locally and systematically [129]. Some studies tried to control the corrosion speed by improving the alloy design, casting conditions, and processing techniques. These efforts could attenuate the corrosion speed to a certain extent, while these methods might potentially weaken the mechanical strength or biocompatibility. Balancing all the factors, surface coating modifications were intensively developed and assessed. Marulanda et al. roughly classified the surface coating techniques as chemical modifications and physical modifications [130]. Chemical modification can be defined as using chemical or electrochemical methods to form a new phase on the metal surface by chemical binding, which involves acid etching, alkaline treatment, fluoride treatment, and anodizing coating. Physical modification can be defined as introducing physical processing techniques or new adhesive phases on the metal

surface without chemical binding between the coating and metal substrates, which involves metal oxide implantation, laser surface processing electron beam treatments, and ion implantation. In addition, apatite coatings and organic polymer coatings can be prepared in both chemical and physical methods (Fig. 3).

4.1. Chemical modifications

Acid etching can remove galvanic corrosion inducing impurities, Fe for instance, and processing deformation from material surface [131,132]. Acid etching could form uniform, equal potentialized layers to clear the native and porous oxide films. Turhan et al. reported that H_2SO_4 could enhance AZ91D alloy's corrosion resistance [133]. Gray et al. reported a $Mg_3(PO_4)_2$ film formation after applying phosphoric acid treatment to AZ31 alloys [134]. Supplit et al. compared the corrosion resistance of different acids among acetic, nitric, phosphoric and hydrofluoric acid treatment. They reported acetic and phosphoric acid etching could decrease degradation speed effectively [135]. Besides AZ alloys, Marcjanna et al. used acetic acid etching to remove the surface contamination on Mg-xGd alloys. They reported that the removal of 2–9 μm of material from the surface was sufficient to clean Fe contamination for a plain surface morphology [136]. Alkaline treatment promoted passive layers on the metal surface by soaking the Mg-based metals in an alkaline solution. Lorenz et al. soaked Mg into NaOH solution and found a dense $Mg(OH)_2$ passive layer on the surface of Mg and its alloys. This study reported the passive layer could effectively retard the corrosion speed [137]. Gu et al. heated the Mg–Ca alloys at 773K after soaking them in an alkaline solution, which could control the corrosion rate of less than 20 % as the untreated samples [138]. F is an essential element in the dental and skeletal system. Reacting with hydrofluoric acid, the Mg surface formed a MgF_2 coating. Similar to alkaline treatment, the Mg–F conversion reaction happened when soaking the Mg and its alloys into 40–48 % hydrofluoric acid [138,139]. Carboneras et al. and Yan et al. reported that MgF_2 coating could

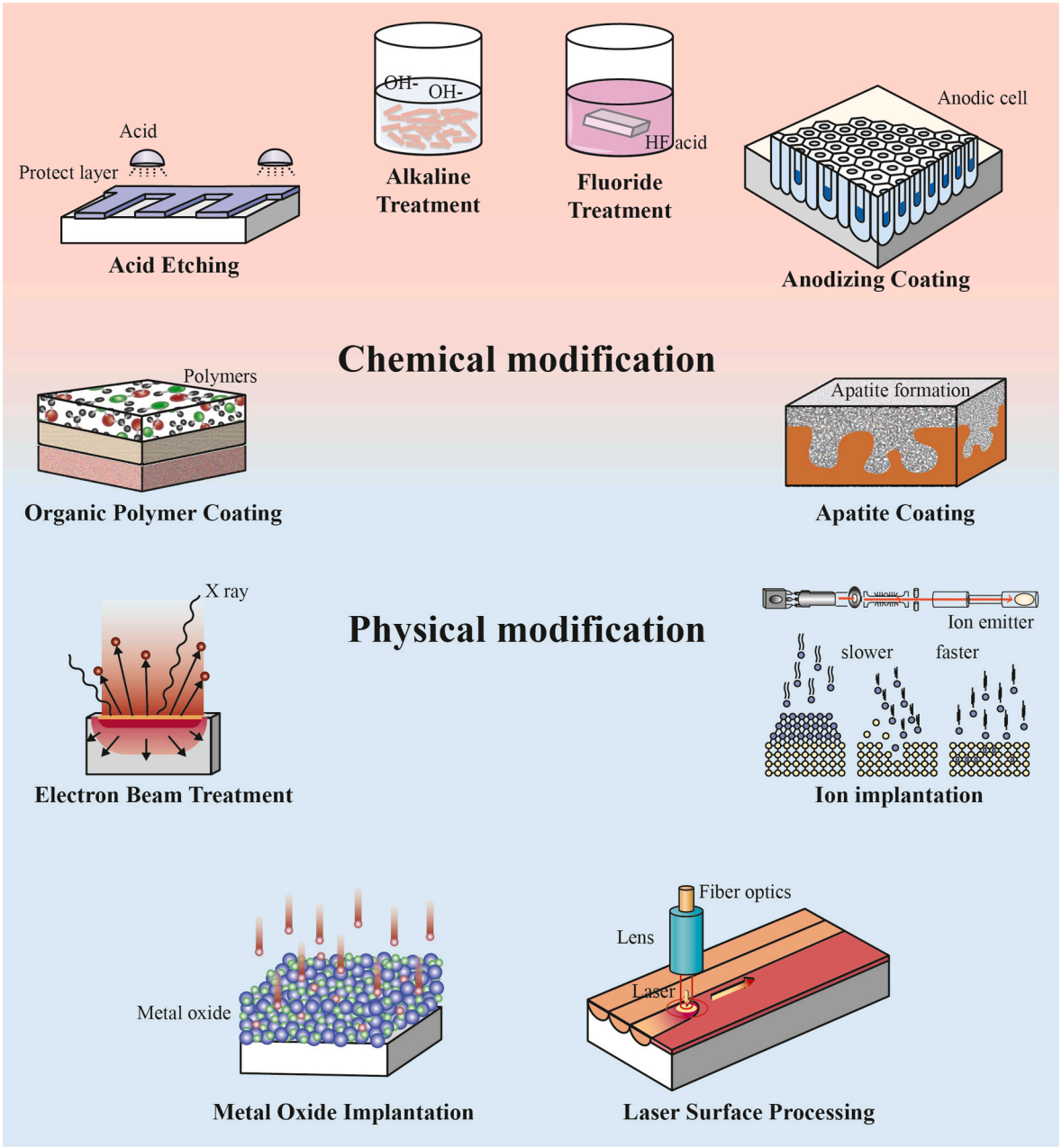

Fig. 3. Surface modification techniques of Mg and its alloys.

effectively delay the degradation speed [140,141]. In the health human body, over 90 % F is stored in skeleton and dental tissue [142]. Excessive intaking F can induce skeletal fluorosis [143]. Disturbed bone turnover finally imbalance the osteogenic and osteoclastic activity [144,145]. Thus, it is crucial to control the releasing speed of F when possessing the coating. Anodizing is an electrolytic process that can convert the metal surface into a durable and corrosion-resistant coating. Zhao et al. assessed the degradation resistance properties of micro-arc oxidation or plasma electrolytic oxidation (MAO) coating on pure Mg [146]. Hiromoto et al. reported that the MAO coating thickness and morphology depended on the increasing voltages [147]. While Gu et al. tested the MAO coating on Mg–Ca alloy with 300, 360, and 400V and reported, samples with 360V presented the best corrosion resistance among all the testing voltages since the microporous formatted inside MAO coating produced 400V [148].

4.2. Physical modifications

Ion implantation is a process that impinging accelerated specific ions into the modified surface. High current pulsed electron beam could modify the surface of metal substrate via high power energy to decrease degradation rate with high efficiency [149]. Unlike the mentioned methods, ion mixing could not form a distinct interface [150]. This character indicated that ion implantation was considered a corrosion resistance strategy at the early degradation stage. Oxygen, nitrogen, and carbon dioxide could passivate the metal surface by Mg–O bonding, Mg_3N_2 formation, and graphite state carbon [151–153]. Unlike gas ion implantation, metal ions involving Zn, Al, Zr, Ti, and Ta implantation were processed by physical techniques such as direct current reactive magnetron sputtering or hydrothermal treatments [154,155]. Considering the excellent corrosion-resistant properties of metal oxide. The dual ion implantation, such as Al_2O_3, TiO_2, ZrO_2, CeO_2, and Cr_2O_3, were applied to enhance corrosion resistance [156–161]. The laser melting technique could enhance Mg–Al alloy corrosion resistance by the Al-composed microstructure [162,163]. Therefore, this technique might prefer to process Mg–Al alloys. The laser shock peening technique could impart compressive residual stresses to improve metal surface integrity, hindering degradation [164]. Both of mentioned laser techniques used neodymium-doped yttrium aluminum garnet (Nd: YAG) laser. The power density, wavelength, scanning speed, frequency, and laser pulse duration still need further investigation.

4.3. Chemical and physical modifications

Hydroxyapatite (HA, $Ca_{10}(PO_4)_6(OH)_2$) is one of the major compositions of a mineralized matrix of bone. As a relatively well-developed coating method, many studies reported that apatite coating presented good osteogenic potential and cell adhesion during fracture healing [165]. Hiromoto et al. used a Ca chelate compound to synthesize the HA with a highly crystallized structure [147]. Enlighted by the chemical modification, Wang et al. and Meng et al. prepared fluorine-doped HA-$_xF_x$ (FHA) coating on Mg–Ca–Zn alloys. This smooth and dense coating offered strong protection to attenuate the degradation speed [166,167]. Hahn et al. developed HA/chitosan coating on AZ31 alloy to improve the corrosion resistance and osteogenic potential [168].

Unlike other modification techniques, organic polymer coatings are an enormous family. This review classified the coating types as synthesized polymer coatings and nature-derived polymer coatings. The synthesized polymer was frequently selected as the coating material because they were easily modified chemically, physically, or mechanically [169,170]. Poly lactic acid (PLA) was initially identified as an ideal material as the surface coating since its good biocompatibility and poor mechanical strength. However, Chen et al. reported that dip-coated PLA presented poor adhesion strength, which failed to protect Mg substrates [171]. To solve the problem, Alabbasi et al. applied a spin coating technique to uniform the thickness of PLA coating to enhance the corrosion resistance of AZ91D [172]. Zeng et al. and Shi et al. further coated PLA on MAO-treated Mg alloys to improve the corrosive resistance significantly [173]. Poly (lactic-*co*-glycolic) acid (PLGA) can degrade into glycolic acid (GA) and lactic acid (LA). The material properties of PLGA can be easily modified by adjusting the ratio of GA and LA [174,175]. Ostrowaski et al. reported the corrosion rate decreased with the increasing PLGA coating thickness after testing different thickness of PLGA coating on AZ31 and MgY_4 [176]. Chen et al. furtherly loaded inhibitor benzotriazole with PLGA. The benzotriazole could be released when PLGA particles reacted with water and pH changing to prevent successive corrosion [177]. Like PLA and PLGA, Polycaprolactone (PCL) also controls the corrosion rate by increasing coating thickness. Degner et al. observed that the corrosion resistance reached tenfold with the PCL concentration from 2.5 to 7.5%w/v [178]. The advantages of natural polymeric coating are their bioactivities and non-immunogenic properties. Chitosan derives from the exoskeletons of crustaceans and the cell walls of fungi [179]. It could decrease the corrosion rate and provide an adhesion basal matrix for cell proliferation [180,181]. Alginate can be extracted from the cell walls of bacteria and brow algae [182]. The structure of alginate allowed cell adhesion on the chemically modified coating [183,184]. Cellulose is rich in the biosphere of various species [185]. Roshan et al. reported cellulose could enhance the mechanical strength of PLA coating [186]. Neacsu et al. reported cellulose could promote cell adhesion, proliferation, and osteogenic differentiation [187]. Hyaluronic acid is one of the components of an extracellular matrix with a poly repeating disaccharide structure [188]. The hyaluronic acid/Ce coating and hyaluronic acid/-carboxymethyl cellulose coating were developed to enhance corrosion resistance [189,190]. Chitin is distributed in the inner cells of arthropods. Chitin coating was initially developed for Zn and Ti implants [191]. Fooladi et al. reported it also could delay the AZ91 degradation [192]. As an anticoagulant, heparin coating or fibroin-blended heparin coating could control metal corrosion and inhibit platelet adhesion [193]. The heparin/carboxymethyl chitosan coating presented good antibacterial activity [194]. Type I collagen coating could promote osteoblast activities around implants through a protein-binding effect [195]. Electrochemical methods could develop serum albumin coating. It could control the corrosion rate by lowering the cathodic current and increasing corrosion resistance [196]. Gelatin is widely dispersed in human tissues. Chan et al. reported that the gelatin coating on $Mg_{67}Zn_{28}C_5$ alloy could present different corrosion resistance behaviors among the degradation products [197]. Mixing with PLGA, the gelatin coating was used to protect the MAO film on WE42 alloys, which formatted a multi-layered defense system [198]. Silk fibrin can present an epithelial state, spun silk state and assembled interfacial silk state to fit different functional demands [199]. The silk fibrin coating could effectively control the release of hydrogen [200]. Since its spun silk state consists of β sheet structure, the silk fibrin coating was designed as a drug delivery system for WE43 stent [201]. Like other natural polymers, the fibrin silk hybrid coating could effectively control the corrosion rate [202]. Phytic acid could chelate the Mg^{2+} to protect the Mg substrate and $Mg(OH)_2$ layer [203,204]. Yang et al. developed a phytic acid/Ce coating that could release carried Ce^{3+} to form a transition film [205]. Stearic acid was also studied to control corrosion resistance due to hydrophobicity [206,207].

5. Biological potential of Mg-based implantation

With the complicated degradation process, biological factors involving Mg^{2+}, calcium phosphate salts, and alkaline environment were produced. These degradation products contributed to bone regeneration via multiple dimensions (Fig. 4).

5.1. Bone-nerve-bone circuit

Zhang et al. found that the Mg^{2+} released from intramedullary nail

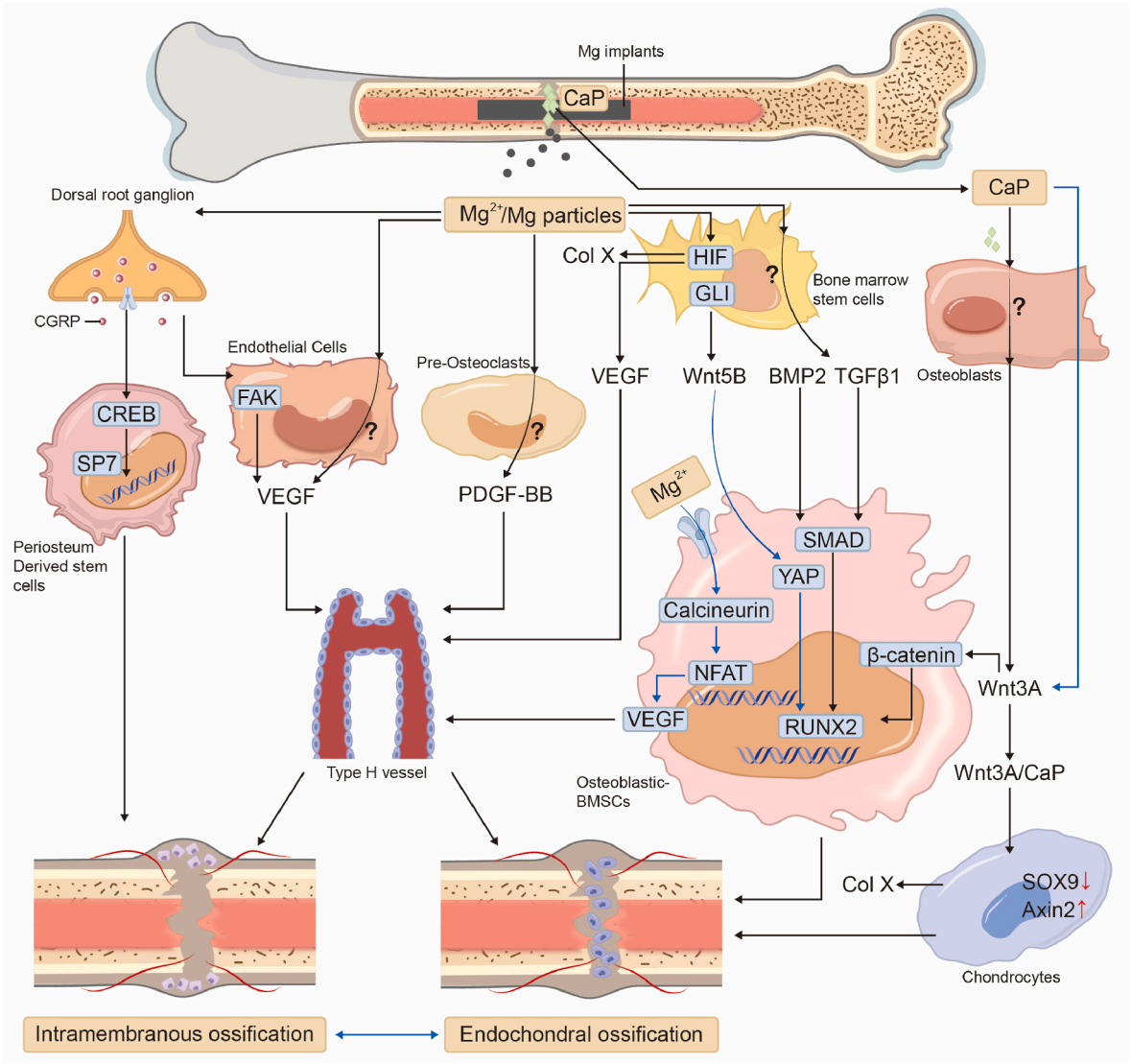

Fig. 4. The synergetic and cross talking net among various Mg degradation triggered osteogenic pathways, CaP: calcium phosphate crystal; CGRP: calcitonin gene-related peptide; CREB: cAMP-response element binding protein; Sp7: Osterix; FAK: focal adhesion kinase; VEGF: vascular endothelial growth factor; PDGF: platelet-derived growth factor; GLI: glioma-associated oncogene homolog; HIF: hypoxia inducible factor; WNT: wingless/integrated; BMP2: bone morphogenetic protein; TGF: transforming growth factor; SMAD: small mothers against decapentaplegic; YAP: hippo/yes-associated protein; NFAT: nuclear factor of activated T cells; SOX: sex determining region Y; RUNX: runt-related transcription factor; Axin: axis inhibitor; symbol "?": the potential mechanisms require further investigation or confirmation.

cavities and fractures move backward along the nerve fibers to the dorsal root ganglion. Mg^{2+} was transported into the dorsal root ganglion through Mg transporter 1 and transient receptor potential cation channel 7, further stimulating the secretion of calcitonin gene-related peptide (CGRP) to activate periosteal stem cells. Therefore, this bone-nerve-bone circuit promoted the formation of new bone at the wound site [208]. This discovery partially explained why Mg^{2+} could not directly promote bone formation *in vitro*, while Mg-based implants could promote bone formation *in vivo*. Tian et al. developed a Mg–Ti metal composite intramedullary fixation system to validate the CGRP osteogenesis theory in a fracture repair model [209]. Zheng et al. used the same intramedullary nail to treat atypical fractures caused by bisphosphonates. They used single-cell sequencing technology to deeply explain that Mg promoted the release of a large amount of CGRP, which effectively inhibits the excessive fibrosis process at the fracture healing site, thereby improving the healing rate of atypical fractures caused by bisphosphonates [210]. In the field of bone defects, Li et al. found that Mg implants can be combined with distraction osteogenesis technology to enhance critical bone defect repair. The primary mechanism is the activation of the CGRP-FAK-VEGF signal axis connecting sensory nerves and endothelial cells by Mg implants [113]. In terms of anterior cruciate ligament reconstruction, Wang et al. reported that secondary suturing of the periosteum around the implanted Mg rod to the tendon graft could significantly promote tendon-bone healing [211].

5.2. Angiogenesis

Mg^{2+} could activate receptors through hypoxia-inducible factor 2a (HIF2a) and peroxisome proliferators in promoting angiogenesisγ (PPAR). The coupling regulation stimulated the secretion of vascular endothelial growth factor (VEGF) [212]. Increased vascular endothelial growth factor (VEGF) could promote the H-type capillaries required for bone formation [213]. Research has reported that high-dose Mg^{2+} could also directly stimulate endothelial cell proliferation and induce angiogenesis [214,215]. Wang et al. reported that inserting the Mg rod into bone marrow could elevate the local platelet-derived growth factor

(PDGF-BB) expression. Yet the derivation of PDGF-BB was not clearly identified. Zhai et al. reported Mg^{2+} could interfere with the activity of osteoclast precursors [216]. Xie et al. reported PDGF-BB was produced by pre-osteoclasts to $CD31^{hi}Emcn^{hi}$ cell to couple angiogenesis and osteogenesis [217]. Further study is required to provide direct evidence to confirm this pathway.

5.3. Osteogenesis

After liquid dilution and refreshment, a moderate alkaline environment could accelerate mineral deposition and weaken osteoclast activity [95,96]. Hamushan et al. found Mg^{2+} activate Gli/Wnt5b/YAP pathway during the bone detraction process [218]. Wang et al. reported that high-purity Mg interference screws enhanced transforming growth factor beta (TGFβ) expression level in anterior cruciate ligament (ACL) reconstruction model [219]. Similarly, Cheng et al. found that Mg interference screws enhanced the secretion of local proteins of bone morphogenetic protein 2 (BMP2) [220]. The local osteogenic effect of Mg had also been extensively studied. Hung et al. found that low concentrations of Mg^{2+} (1 mmol) can activate the Wnt signaling pathway in bone marrow-derived stem cells (BMSCs), thereby improving the expression of beta-catenin, LEF1, and Dkk1 [221]. Mg^{2+} (1 mmol) could also upregulate adhesion α5β1 [219] and adhesion kinase pathway [222] to improve the local adhesion ability of BMSCs. On the contrary, some studies reported that Mg^{2+} could not promote *in vitro* osteogenesis [223,224], while metal extracts could stimulate the formation of Ca nodules [209]. To investigate the potential mechanism behind this divergence, He et al. observed the Mg was replaced by calcium phosphate progressively by Scanning Electron Microscope and Energy Dispersive Spectroscopy (SEM/EDS). The accumulated calcium phosphate promoted local endochondral ossification via upregulating Wnt3a expression. Similarly, this key finding was confirmed *in vitro* experiment by comparing the osteogenic potential among Mg^{2+}, Mg metal extraction, and Mg^{2+} mixed with calcium phosphate [62].

6. Preclinical test of Mg-based implants

Animal experiments played an important role in assessing the safety and biological activity of Mg implants. The animal model of Mg-based implants mainly involved fracture repair and anterior cruciate ligament reconstruction (Table 2). Zhang et al. elucidate the Mg^{2+} derived from intramedullary nail could trigger dorsal root ganglion releasing CGRP to mediate fracture healing [208] (Fig. 5A). Han et al. used pure Mg screws to fix femoral intra-articular fractures and found that compared to PLA screws, more bone tissue can grow at the fracture site [225] (Fig. 5B). Chaya et al. used Mg screws and metal plates to fix ulnar fractures in a rabbit model. Since the rabbit's upper limbs did not bear weight, researchers observed better healing and more bone formation with the Mg-based plates degraded [226] (Fig. 5C). To avoid early internal implant fracture, Jähn et al. reported that using Mg–Ag alloy intramedullary nails to fix femoral shaft fractures found that the intramedullary nails still showed a complete internal fixation structure and strength in the early stage of degradation. A larger callus was found at the fracture site in the Mg implantation group, and mechanical tests also confirmed that the Mg implantation group had better compressive strength [227] (Fig. 5D). To slow down the mechanical corrosion of the screw plate interface, Tian et al. sprayed PLA coating on the tail of the Mg screw. In the Z-shaped fracture model, the Mg screw protected by the coating stably degraded, prolonging the integrity of the mechanical structure to some extent, and the slower degradation rate also reduced the accumulation of hydrogen gas [209] (Fig. 5E). Bisphosphate salts were taken to treat osteoporosis, which might occur atypical fracture. Over-fibrosis at the fracture site could interfere bone growth. Zheng et al. developed a Mg-stainless steel hybrid IMN to promote CGRP release, which could suppress the fibrosis via targeting on the sorting gene by single cell sequence analysis [210] (Fig. 5F).

In the field of sports medicine, Cheng et al. reported that Mg interference screws could increase the levels of BMP2 and VEGF at the tendon-bone healing interface [220] (Fig. 6A). Meanwhile, they also reported that Mg screw degradation could inhibit bone resorption and

Table 2
Preclinical test of Mg-based implants in trauma.

Materials	Implants	Control	Models	Animals	Main findings and mechanism
HP Mg [208]	IMN screw	SS	Femur shaft fracture	Rat	Mg^{2+} promoted CGRP-mediated osteogenic differentiation
HP Mg [225]	Screw	PLA	Distal femur fracture	Rabbit	Promote OPN and Runx2 expression to stimulate new bone formation
HP Mg [226]	Screw/plate	Ti	Ulna fracture	Rabbit	New bone formation at non-weight bearing site
Mg-Ag [227]	IMN screw	SS	Femur shaft fracture	Mice	Larger callus and higher ultimate loading
Coating Mg [209]	Screw	Ti	Femur shaft fracture	Rabbit	More controllable degradation continuously stimulated CGRP release to form larger callus
HP Mg [210]	IMN screw	Ti	Bisphosphonate fracture	Rat	Mg^{2+} activated downregulated CGRP releasing to block extracellular fibrosis at fracture site
HP Mg [228]	Interference screw	Ti	ACL reconstruction	Rabbit	Downregulated MMP13 to reduce bone and tendon graft resorption
HP Mg [220]	Interference screw	Ti	ACL reconstruction	Rabbit	Modulated VEGF and BMP2 expression to benefit fibrocartilages regeneration
HP Mg [229]	Interference screw	Ti	ACL reconstruction	Rabbit	Mg degradation mineralized bone tendon attachment as Sharpy like fiber
HP Mg [219]	Interference screw	Ti	ACL reconstruction	Rabbit	Mg degradation promoted tunnel bone MAR by elevating TGFβ1 and PDGF BB expression
Mg-Zn-Sr [102]	Interference screw	PLA	ACL reconstruction	Rabbit	Mg degradation stimulated bone growth into tunnel
HP Mg [230]	Ring	Suture	ACL Repair	Goat	Better knee function
Mg-Zn-Gd [62]	Wire	Suture	ACL reconstruction	Rabbit	Mg wire degradation balanced bone growth and fibrocartilage formation via dynamically regulating Wnt3a, VEGF, BMP2
HP Mg [231]	Wire	Suture	Rotator cuff repair	Rat	Fibrocartilage bone tendon junction formed at suture site
HP Mg [232]	Wire	Suture	Meniscus repair	Rabbit	Promote synovial derived stem cells presenting chondrogenesis to form cartilage and fibrocartilage
HP Mg [233]	Suture anchor	Bio-composite	Rotator cuff repair	Sheep	Good anchoring function with better intra-tunnel healing
HP Mg [113]	IMN	SS pin	Bone distraction	Rat	Blood vessel growth and bone growth with detraction via CGRP-FAK-VEGF pathway
HP Mg [234]	IMN	SS pin	Bone distraction	Rat	More bone growth with detraction via Gli/Wnt5b/YAP pathway
HP Mg [235]	IMM	SS pin	Bone distraction	Rat	Mg^{2+} suppress VHL and secondarily elevated VEGF expression to enhance angiogenesis and osteogenesis

HP: high purity; IMN: intramedullary nail; Ti: Titanium; PLA: polylactic acid; SS: stainless steel; MAR: mineralized rate; ACL: anterior cruciate ligament.

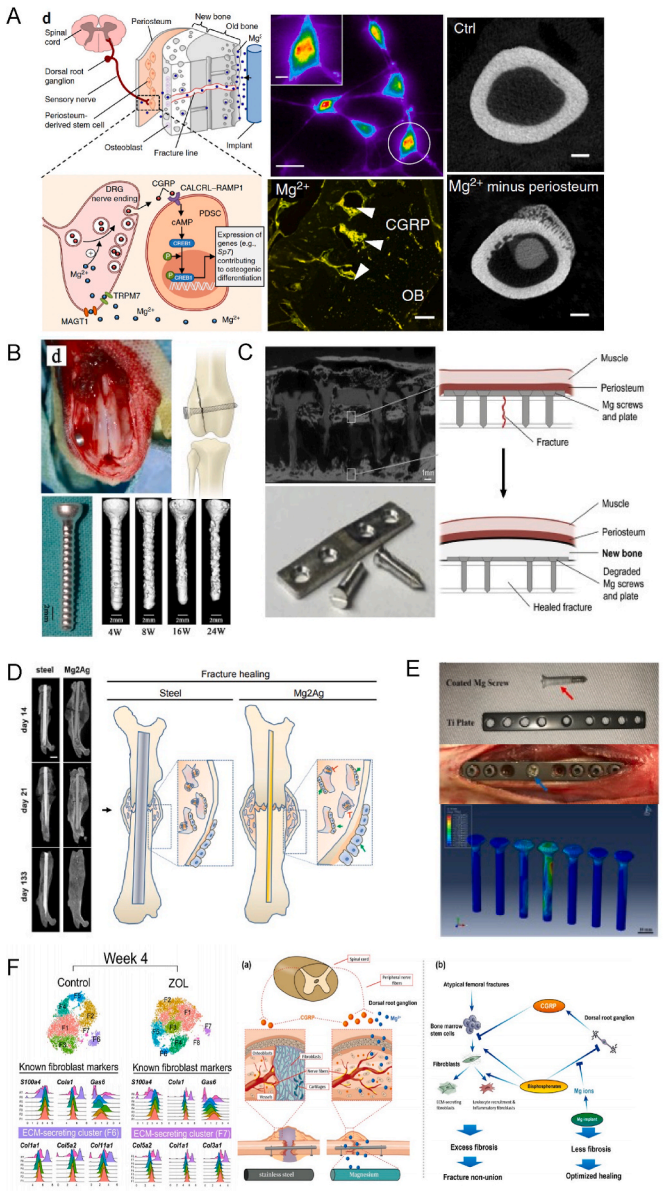

Fig. 5. Mg implants application in fracture fixation, A. Mg^{2+} from IMN triggered CGRP releasing to promote osteogenesis, Zhang et al. [208], copyright 2016, Springer Nature; B. Mg screw fixed distal femur fracture, Han et al. [225], copyright 2015, ELSVIER; C. Mg screw and plate fixed ulna fracture, Chaya et al. [226], copyright 2015, ELSVIER; D. Mg–Ag alloy IMN fixed femur shaft fracture, Jähn et al. [227], copyright 2016, ELSVISER; E. coated Mg screw fixed femur shaft fracture, Tian et al. [209], copyright 2018, ELSVISER; F. Mg^{2+} form IMN triggered CGRP releasing to suppress local fibrosis to promote atypical fracture healing, Zheng et al. [210], copyright 2022, ELSEVIER.

tendon graft atrophy via suppressing MMP13 expression, which effectively enhanced the mechanical strength of bone tendon junction at the earlier healing stage [228]. Wang et al. found that Mg alloy interference screws can improve TGFβ1 and PDGF-BB level in the early stages to improve the bone formation around the tunnel [219] (Fig. 6B). He et al. demonstrated Mg wire degradation regulate and balance osteogenesis and chondrogenesis to reconstruct fibrocartilage connection between tendon and bone [62] (Fig. 6C). In addition to promoting bone formation, Ferraro et al. used Mg metal rings to repair ruptured anterior cruciate ligament and reported that Mg degradation can promote tendon and ligament healing [230] (Fig. 6D). Besides, Zhang et al. embedded U-shaped Mg wire at tibia platform to activate stem cells potential to promote meniscus regeneration [232] (Fig. 6E). In shoulder surgery, Chen et al. developed an Mg suture anchor to fix the tendon through the bone tunnel and assessed its biological effects and safety in large animal [233] (Fig. 6F). Zhang et al. applied Mg wire to repair the rotator cuff and reported a layered fibrocartilage bone tendon healing, which could potentially reduce the re-tear rate [231] (Fig. 6G).

In bone defect repairing, Li et al. used Mg intramedullary nail to promote healing effect of bone extraction via CGRP-FAK-VEGF axis (Fig. 7A). Compared to CGRP-FAK-VEGF pathway, Hamushan et al. demonstrated Mg^{2+} could suppress VHL expression and indirectly triggered HIF-1α-VEGF pathway [235] (Fig. 7B). They also reported Mg could upregulate Wnt5b to promote local bone formation with same animal model [234] (Fig. 7C). These three key studies comprehensively indicated the potential synergetic effect between angiogenesis and osteogenesis during bone detraction process. In this process, Mg degradation played a crucial role.

7. Clinical study of Mg implants

Advance to animal assessments, some clinical studies have been processed. Zhao et al. and Sun et al. applied Mg screw to fix the bone graft in femur head necrosis [236,237] (Fig. 8A and B). Since the pathology of femur head necrosis potentially attribute lacking blood supply and bone resorption were key points in disease progress, the Mg degradation triggering angiogenic and osteogenic potential successfully retarded femur head collapse to leave time and space for tissue regeneration. Windhagen et al. developed the MAGNEZIX® screw to treat hallux valgus [238] (Fig. 8C). Due to no obvious gas emission and implant fracture were observed in clinical follow-up, this screw honored as the first approved Mg-based implant in orthopaedics. Following this fundamental medical translation, Lee et al. observed the process of new bone tissue replacing Mg screw when fixing distal radius fracture [63] (Fig. 8D). Xie et al. developed Mg-Nd-Zn-Zr alloy (JDBM) screw to fix medial ankle fracture. Compared to pure Mg screw, JDBM screw presented a more controllable degradation speed without gas accumulation [239] (Fig. 8E). These clinical studies demonstrated the promising future of Mg implants, which might encourage colleagues to accelerate the translational work. Still, this review highlighted that all the clinical studies must be based on sufficient evidence from lab side and must pass the ethical review.

8. Prospects for biological matching spine fusion cage development

8.1. Background of lumber intervertebral fusion

More than 1 billion people worldwide are suffering from lumbar spondylosis, and approximately 600,000 patients in the United States require lumbar spine surgery each year [240]. In China, according to incomplete statistics from healthcare institutions, the number of patients with lumbar spine diseases has exceeded 200 million, and there are over 1 million cases of lumbar spine surgery each year. In the surgical treatment of lumbar spine diseases, lumbar fusion surgery is mainly suitable for cases of lumbar spondylolisthesis, lumbar disc disease combined with segment instability, segment instability after nerve decompression, lumbar spinal stenosis combined with degenerative scoliosis or kyphosis, as well as recurrent lumbar disc herniation or lumbar spinal stenosis requiring reoperation [241].

Posterior spinal fusion can be divided into posterior lateral and intervertebral fusion [242]. Summarizing the clinical experience of two fusion strategies, posterior lateral fusion is relatively simple to operate and can be directly reinforced on the lateral side of the decompression segment. However, for cases where nerve root outlet decompression is relatively thorough, there is often insufficient space for posterior lateral bone grafting. In addition, due to the relatively small operating space between the nail cap of the pedicle screw and the paraspinal muscle tissue, cortical removal is often relatively difficult, which induces bone

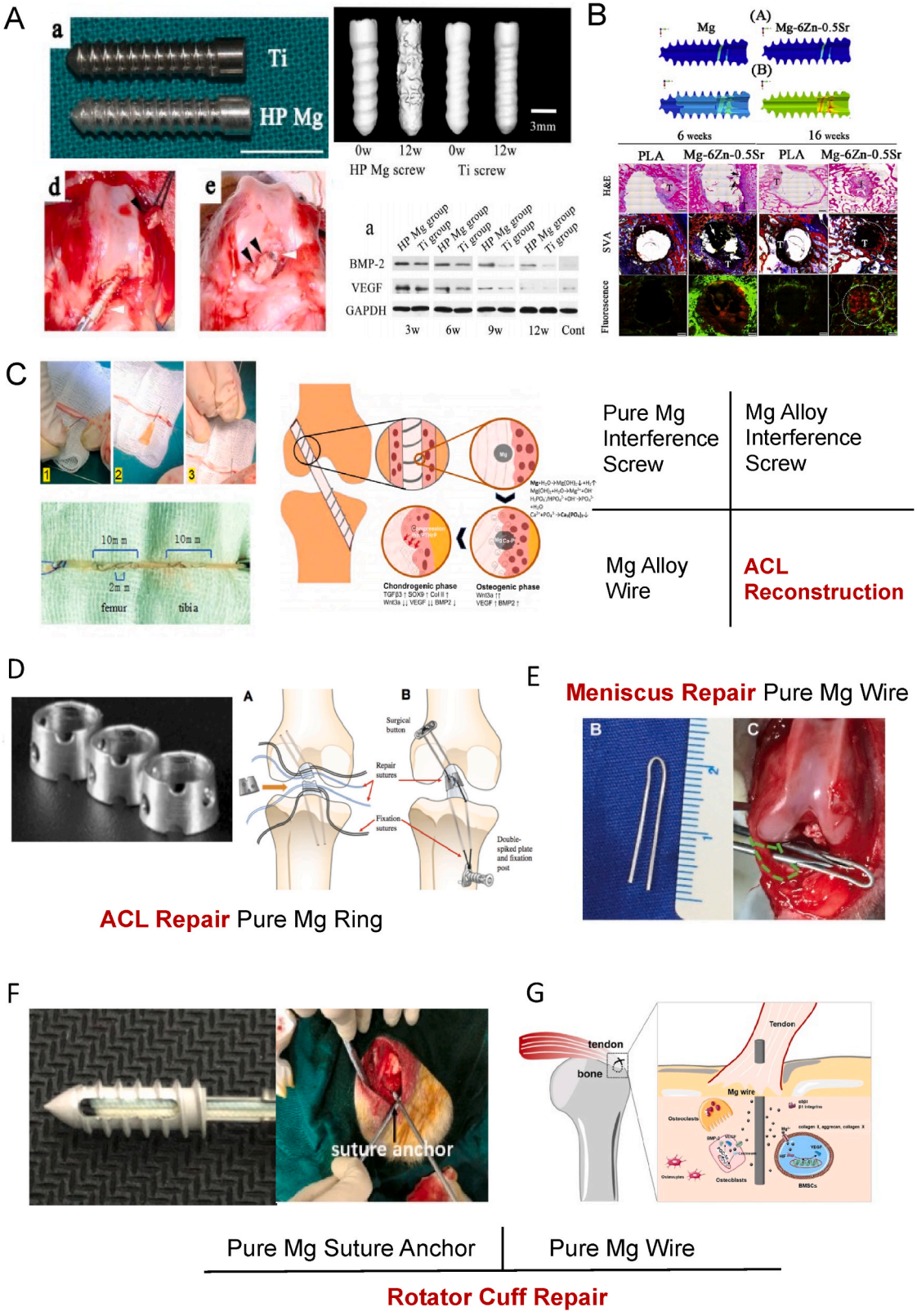

Fig. 6. Mg implants application in sports medicine, A. Mg interference screw promoted bone tendon healing via upregulating BMP2 and VEGF expression, Cheng et al. [220], copyright 2016, ELSEVIER; B. Mg–Zn–Sr alloy interference screw promoted tunnel healing, Wang et al. [102], copyright 2018, ELSEVIER; C. Mg–Zn-Gd alloy wire suture tendon graft mediated fibrocartilages regeneration, He et al. [62], copyright 2024, Ke Ai, Creative Commons Attribution License; D. Mg ring repaired ACL rupture, Farraro et al. [230], copyright 2016, Wiley, free access; E. Mg wire enhanced meniscus regeneration, Zhang et al. [232], copyright 2019, SAGE; F. Mg suture anchor to enhanced bone tendon healing for reducing rotator cuff re-tear rate, Chen et al. [233], copyright 2022, ELSEVIER, Creative Commons Attribution License. G. Mg wire repaired teared rotator cuff, Zhang et al. [231], copyright 2022, ELSEVIER, Creative Commons Attribution License.

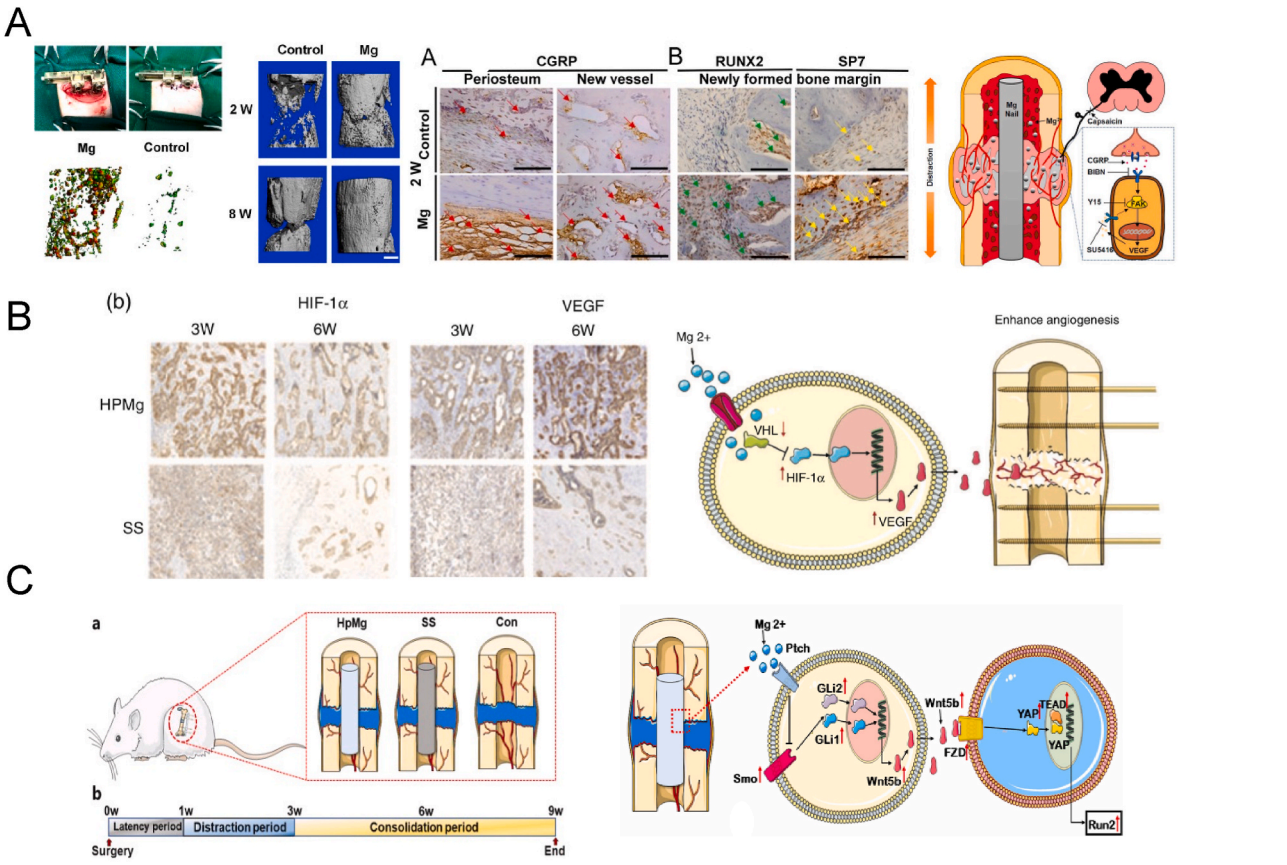

Fig. 7. Mg implants application in bone distraction, A. Mg^{2+} from IMN enhanced H type vessel formation with detraction process via CGRP-FAK-VEGF axis, Li et al. [113], copyright 2021, ELSEVIER; B. Mg IMN degradation elevate HIF-1α and VEGF expression to facilitate bone formation via inhibiting VHL, Hamushan et al. [235], copyright 2020, SAGE; C. Mg IMN degradation upregulated Wnt5b expression to promote osteogenesis with detraction, Hamushan et al. [234], copyright 2021, KE AI, Creative Commons Attribution License.

grafting interface may not be fully exposed. Compared to posterior lateral fusion, intervertebral fusion has a larger fusion interface area, and using an endplate scraper can effectively remove lumbar discs and cartilage that can hinder bone fusion. intervertebral fusion can also maintain the anterior column height for patients after removing intervertebral discs [243]. The commonly used clinical method for intervertebral fusion is to implant a spinal fusion cage containing fragmented bone blocks into the intervertebral space. Although the vast majority of cases can achieve satisfactory intervertebral fusion, there is still a considerable proportion of cases with unsatisfactory intervertebral fusion [244].

The ideal bone fusion requires an active osteogenic environment, space for new bone growth, and stable mechanical support. If the surgical segment cannot form effective bone fusion, pseudoarthrosis will form between segments, and repeated movement can lead to internal fixation failure and symptom recurrence [245]. Many reasons lead to unsatisfactory fusion, and one of the main reasons is the defect in the material characteristics of the fusion device [246]. Therefore, the materials of spinal fusion devices have been continuously developed in recent years, from initially considering only the osteogenic activity or mechanical properties of the materials to proposing a design concept that balances osteogenic activity and mechanical matching, and finally incorporating biodegradable metals into the research and development of fusion devices. In today's rapidly advancing field of materials science and medical cognition, the design ideas, research, and development niche for biological matching spinal fusion devices that truly balance biomechanical matching, biodegradation matching, and biological osteogenesis matching are gradually becoming clear.

8.2. *Different lumbar fusion cages in clinical application*

Although spinal fusion cages have been widely used in spinal surgery for years, the fusion rate was not satisfactory since the limitations of different cages [244] (Table 3). Traditional Ti-based fusion cages presented a relatively satisfactory fusion rate after surgery. Still, due to the substantial mechanical strength of hard metals, the incidence of fusion cage subsidence remained high [11,247] (Fig. 9A and J). PEEK-based fusion cages could significantly reduce the cage subsidence incidence because its mechanical properties were close to bone. However, PEEK material presented poorer bone induction and a lower fusion rate than Ti-based fusion cages (Fig. 9B and J). Wrangel et al. reported the fusion rate of cases using Ti cage was 53 % while cases using PEEK cage was only 32 % in a 2-year-follow-up study [248]. Implanting with bone grafts, Cabraja et al. reported the fusion rate between Ti cage group and PEEK cage group was 79.6 %–62.9 % [249]. Seaman et al. concluded the point that PEEK cage presented lower cage subsidence rate while it also presented a lower fusion rate compared to Ti cage by a meta-analysis [11]. To combine the good mechanical properties of PEEK and the active biological potential of Ti together, the hybrid cage that constructed by PEEK interface and Ti subject was developed [250]. However, the fusion rate of Ti-PEEK cage was still not exceeding the Ti cage or PEEK cage [251]. It was attributed that the PEEK particles from wear interface could lead bone resorption [252]. Other than Ti and PEEK, Ta was applied as the material of fusion cage (Fig. 9C). Høy et al. and Kelft et al. reported an over 90 % fusion rate by RCT studies [253,254]. However, Lebhar et al. concerned that the artifacts induced by Ta under CT scanning were significantly stronger than Ti, which might be difficult to identify the fusion level [255]. Recent years, Carbon-Fibere

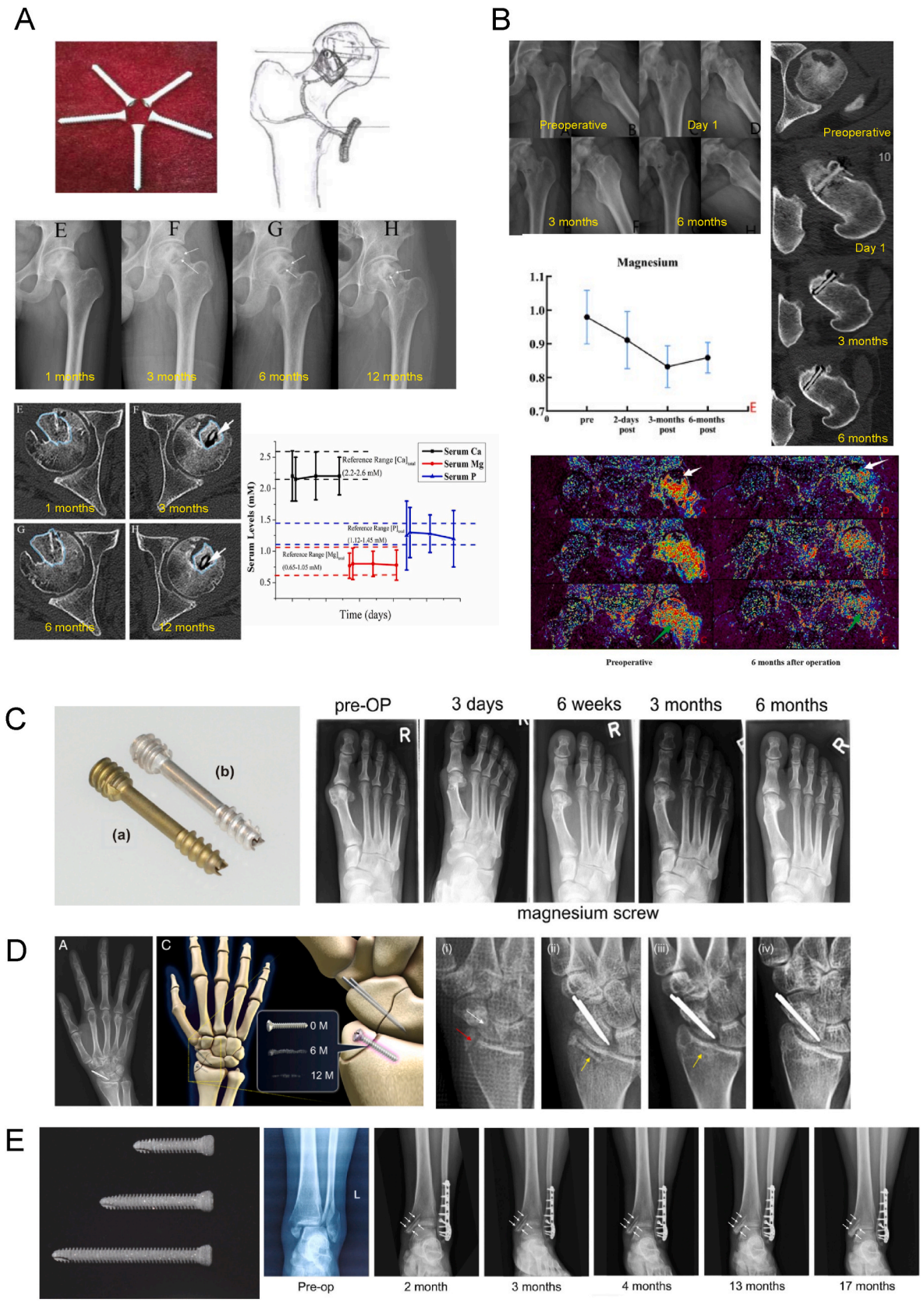

Fig. 8. Mg implants application in clinical scenario, A. 1-year-follow up study observed Mg screw fixed bone slides to treat femur head necrosis, Zhao et al. [236], copyright 2016, ELSEVIER; B. 6-month-follow up study observed Mg screw fixed bone slide to treat femur head necrosis, Sun et al. [237], copyright 2023, Wiley, open access; C. MAGNEZIX® screw applied for hallux valgus surgery, Windhagen et al. [238], copyright 2013, BMC, Creative Commons Attribution License; D. Mg screw fixed distal radius fracture, Lee et al. [63], copyright 2016, PNAS, open access; E. Mg JDBM alloy screw fixed medial ankle fracture, Xie et al. [239], copyright 2016, ELSVIER, Creative Commons Attribution License.

Table 3
Representative spine fusion cages in Chinese market.

Registration certificate name	Materials	Global/ Native	Brand name
INNESIS CAGE	Ti alloys	global	BK
Spine Interbody fusion cages	PEEK	global	BRICON
Spine Interbody fusion cages	PEEK	global	Ulrich
Multi porous metal spine Interbody fusion cages	Ti alloys	native	AKEC
Prospace PLIF System	Ti alloys	global	B. Braun
PROSPACE PEEK PLIF System	PEEK		
TSPACE PEEK Facelift Transforaminal Lumbar Interbody Fusion System	PEEK		
Spine Interbody fusion cages	PEEK	native	Trauson
Spine Interbody fusion cages	PEEK	native	Fule
Spine Interbody fusion cages	Ti alloys		
Spine Interbody fusion cages	PEEK	native	Waston
Anterior Lumbar Cage	PEEK	global	Zimmer
Spine fusion cages, TM Ardis	Ta		
Lateral Lumbar Cage	PEEK		
Zyston Interbody Spacer System	PEEK		
Spine Interbody fusion cages	Ti	native	KANGLI
Spine Interbody fusion cages	PEEK		
Spine Interbody fusion cages	PEEK	native	Liberer
Spine Interbody fusion cages	Ti alloys		
CRESCENT Spinal System	PEEK	global	Medtronic
Capstone Spinal System	PEEK		
Clydesdale Spinal System	PEEK		
Pulse Cage System	PEEK	global	Johnson &
Minimal Invasive Surgery Cage	CFRP		Johnson
Spine Interbody fusion cages, OPAL	PEEK		
Cage System	CFRP		
Spine Interbody fusion cages, T-PAL	PEEK		
Spine Interbody fusion cages	PEEK	native	Sanyou
Spine Interbody fusion cages, AVS Navigator PEEK Spacer	PEEK	global	Stryker
OIC System Implants	PEEK		
Spine Interbody fusion cages	PEEK	global	Spineway
Spine Interbody fusion cages	PEEK	global	GS
Spine Interbody fusion cages	PEEK	native	WEGO
Spine Interbody fusion cages	Ti alloys	native	Walkman
Spine Interbody fusion cages	PEEK		
Spine Interbody fusion cages	PEEK	native	XInrong Boerte
Spine fixation device	Ti alloys	native	YOUBETTER
Spine Interbody fusion cages	PEEK	native	ZhengTian
Brands involved in the table registered at least two types of spine fusion cage in Chinese Market			

Reinforced Polyether Ether Ketone (CFRP) was applied as a replace material of PEEK for cervical, thoracic and lumber intervertebral fusion [256] (Fig. 9D). A multicenter study reported that CFRP-based cage presented good biocompatibility and low loosening rate. However, the fusion rate of CFRP-based cage was still lower than 50 % [257]. Hydrosorb cage was proved to process clinical trial based on excellent lab data. Unfortunately, the clinical translation was finally aborted because the severe bone resorption induced by cage degradation [258] (Fig. 9E and J). Liu et al. developed a polycaprolactone/beta-tricalcium phosphate cage and reported a 14.3 % grade I fusion rate after 6 months and 52.3 % grade I fusion rate after 1 year [259] (Fig. 9F). The major concerning of this cage is if the distributed particles can induce bone resorption, similar to the situation of Ti-PEEK cage and hydrosorb cage. More studies and multi-center RCT are required.

8.3. Development of mechanical matching and biological matching cage

The beginning of biological matching cage development merely focused on morphological matching. Using 3D printing techniques, Liu et al. achieved the first printed tumor prothesis implantation in spine in 2014 [260]. Besides macro structure 3D printing, microstructure 3D printing is also constantly developing. The bonding strength and biocompatibility of the implant-bone interface have long been a concern for orthopedic doctors. Smooth metal interfaces cannot provide sufficient bonding force, and there is no space for bone tissue growth. The porous interface structure forms a mutually embedded structure and ensures the space for tissue growth [261]. As 3D printing technology matured, combining surface treatment technology with 3D printing, cages with integrated macro-microstructures can be printed directly. With this technique, Liu et al. developed a Ti6Al4V-based cage with a trabecular structure to improve spine fusion compared to pure Ti metal and PEEK material [262,263].

In the traditional concept, implant materials with higher mechanical strength should be used to maintain local mechanical strength stability. With an understanding of the relationship between mechanical stimulation and bone metabolism, the drawbacks of the traditional concepts are gradually emerging [264,265]. In the early healing stages of healing, high-strength material implants may directly cause local iatrogenic fractures such as endplate fracture and pedicle fracture, affecting postoperative tissue healing. In the later healing stage, the stress shielding effect caused by high-strength internal implant materials weakens the mechanical stimulation, which induce cage subsidence and non-fusion [266]. Northcutt et al. developed a fusion cage to reduce the negative effects caused by high strength material by matching material density to bone density (US 10779954 B1). However, bone density was not related to mechanical properties, which meant this cage only presented similar bone density [267]. In 2019, through interdisciplinary research with materials science, biomechanics, and machine learning, Li et al. proposed the "Structure-Density-Strength" (SDS) theory and initiated the project of developing biomechanical matching and bio-osteogenic matching spinal fusion cage (the first funding shown in declaration of competing interest). Based on this novel theory, Li et al. applied the patent of biomechanical matching and bio-osteogenic matching spine fusion cage in 2020 (CN 112353530 A) and developed the first-generation of biomechanical matching spine fusion cage (Ti6Al4V) (Fig. 9G). Furthermore, Li et al. integrated artificial intelligence planning and 3D printing technology to optimize the macro and microstructure of the material which could match the bone density distribution of the patient's bony endplate to achieve individualized optimal mechanical strength of the fusion cage [267]. This technology dramatically reduced the material modulus by optimizing the structural design while retaining the osteogenic potential of the Ti alloy prosthesis. Using AI technology, the structure with the highest strength was selected as the final structure among all possible structures with the same modulus [266]. After long-term preclinical testing, the new generation of biomechanical matching lumbar fusion cage, Osteo Match (Ti6Al4V), was approved by CFDA and applied in the clinical scenario (Fig. 9H). In 2022, Wang et al. design a morphological-mechanical matching cage that could distribute the body weight on a larger area [268]. One major concern of this cage was that anterior cervical fusion model in sheep made this large-size cage be implanted into vertebral space. It needs re-design for posterior intervertebral implantation to avoid dual and nerve root injury.

8.4. The prospect Mg-based spine fusion cage R&D

Based on mechanical matched cage, development of biological matching spine fusion cages involving biomechanically matching, biodegradation matching, and bio-osteogenic matching become the next target. Considering the perspectives of mechanical strength and osteogenesis, Mg presents promising translational potential. Moreover, Mg has potential in biomechanical matching in the time dimension because the elastic modulus of fusion bone mass usually changes after surgery. Unlike the area of fracture, sports medicine and bone defects, only limited number of teams developed biodegradable Mg alloy fusion cages to enhance osteogenic potential [269–271]. Although animal experiments reported that Mg-based fusion cages could improve bone formation with a certain mechanical supporting, there is still a long way to go in the process of clinical translation [55] (Fig. 9I and J). Firstly, Mg and its alloy presented low compressive yield strength which can hardly withstand the high pressure between vertebrae. Implants fracturing at

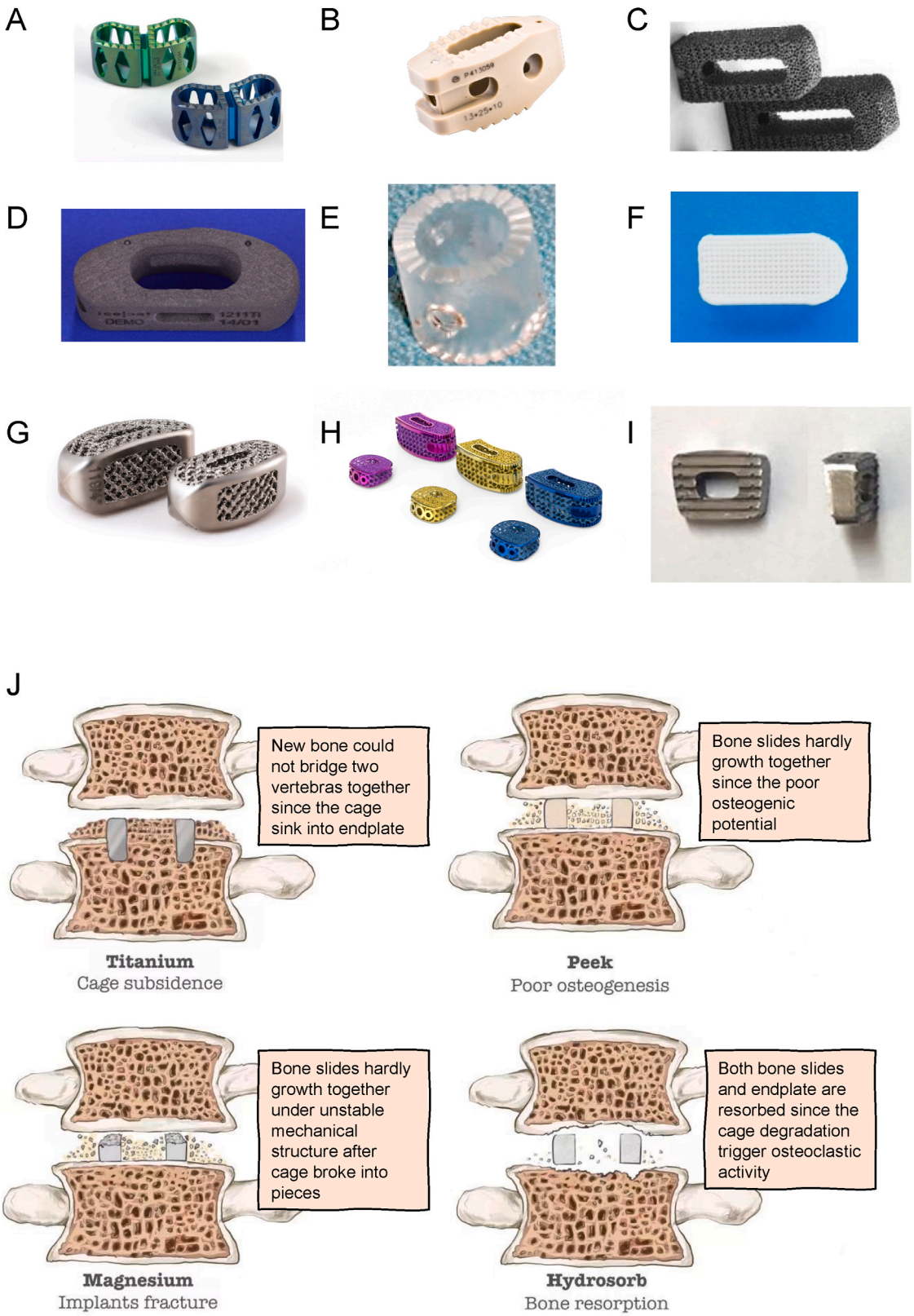

Fig. 9. Development and limitation of lumbar interbody fusion cages, A. Ti cage; B. PEEK cage; C. Ta cage, Lebhar et al. [255], copyright 2020, ELSEVIER, Elsevier user license; D. Carbon-Fibere Reinforced Polyether Ether Ketone (CFRP) cage, Burkhardt et al. [256], copyright 2021, ELSEVIER; E. Hydrosorb cage, Laubach et al. [258], copyright 2022, ELSEVIER; F. Polycaprolactone/β-tricalcium phosphate cage, Liu et al. [259], copyright 2023, WILEY, Creative Commons Attribution License; G. first generation of biomechanical matching cage (Ti6Al4V); H. Osteo Match cage (Ti6Al4V); I. Mg cage, Guo et al. [271]. copyright 2020, ATM, Creative Commons Attribution License; J. the disadvantages of different cages potentially failing in spine fusion.

the early healing phase seriously jeopardize clinical safety. Secondly, larger Mg metal implants may accumulate more degradation byproducts in the body (such as hydrogen and alkaline environments), which, to some extent, can also jeopardize clinical safety. In addition, Yang et al. reported that Mg may be more inclined to regulate bone resorption in the late degradation stage, thus long-term degradation may not benefit local osteogenesis [272].

Balancing the biological characteristic and limitations of Mg-based implants, the Mg hybrid cage was considered as a reasonable direction of spinal fusion cage design. Our team has developed the first-generation of Mg-PEEK fusion cage and the second-generation product development is in progress. The PEEK main body support the mechanical loading constantly, while embedded Mg wire activate the osteogenic potential to improve bone fusion. The embedding design also protect nerve root from degradation products and Mg particles, which can also prevent the ectopic ossification to compress nerve root and cauda equina (Fig. 10A and B). Zhang et al. [208] and Zheng et al. [210] developed a Mg–Ti hybrid intramedullary nail to fix long bone fracture. Similar design may be applied in Mg-PEEK cage or Mg–Ti cage. According to the requirement of FDA, *in vivo* assessments play crucial role in translation process. Our first-generation Mg-PEEK cage has completed cadaver implantation test (Fig. 10C). The Mg-PEEK cage can be implanted into the cervical intervertebral space without Mg wire breakage. Although some studies used rats and rabbits as the spine fusion model, the goat/sheep cervical spine fusion model is better for intervertebral fusion. The most advantage of goat/sheep model is the cervical alignment is relatively vertical to the ground, which is similar to the mechanical environment of human spine.

When designing the Mg-PEEK cage, different forms of Mg were tested and compared. Using Mg particles embedding into PEEK presented high corrosion rate with large volume of hydrogen emission. While an intact Mg slice covering the PEEK hindered the new bone growth into the cage. Considering all the facts, Mg wire is the optimal and feasible choice. Mg wire presented high formability to fit the morphology of the cage with sufficient strength to keep intact during cage implantation. More importantly, our previous research found that compared to larger implants, Mg wire degraded and promoted endochondral osteogenesis in the early healing stages. Regarding safety, due to the lower amount of wire used than screws or other implants, the amount of hydrogen accumulation was low. In history, Mg-based metal wire was first used in ovarian resection and anastomosis surgery [273]. Although there are some positive effects, Mg-based metal wires exhibit poor mechanical properties even before degradation [273,274]. With improved industrial technology, Mg-based wire materials could be manufactured through the cold drawing process. Compared with the extrusion method, their mechanical properties were significantly enhanced [275]. These Mg wires were further processed into hemostatic clips or stents and were widely used in the fields of cardiac surgery [276] (Fig. 11A), general surgery [277–279] (Fig. 11E–G), neurosurgery [280] (Fig. 11B), urology [281,282] (Fig. 11C and D) and orthopaedics [62,283] (Fig. 11H and I). In the future, using coating modifications and 3D printing, more and more Mg hybrid cages will be developed. We believe the optimal Mg hybrid biological matching spine fusion cage can be developed and benefit patients in the foreseeable future.

9. Summary

Mg's mechanical properties, degradation behaviors, and osteogenic activities indicate that Mg and its alloys are promising biological matching materials for muscular-skeleton system repair and regeneration. However, the collapse of mechanical strength and gas accumulation significantly limited the clinical application of Mg-based implants during the past decades. Novel alloy designs, new processing techniques, and surface modifications improved these implants' mechanical properties and corrosion resistance. Meanwhile, the complicated biological mechanisms of Mg have been extensively unmasked. Based on these new theoretical and practical breakthroughs, more and more pre-clinical studies and clinical trials are being conducted in fracture fixation, soft tissue repair, bone defect regeneration, and femur head necrosis treatment. Considering the mechanical loading of intervertebral space and the risk of spine surgery, the Mg-based cage in spine fusion is still challenging. The authors proposed an Mg-PEEK hybrid design to integrate high mechanical loading and biological activity. Overall, the clinical translation of Mg-based implants is a multidisciplinary task. The primary motivation for composing this review is to promote magnesium-based implants to readers from different professions. This review aims to increase interest in charmful metal and share knowledge and techniques to solve challenges together.

CRediT authorship contribution statement

Xuan He: Writing – review & editing, Writing – original draft, Methodology, Funding acquisition, Conceptualization. **Ye Li:** Writing – original draft, Visualization, Validation. **Da Zou:** Writing – review & editing, Validation, Funding acquisition, Conceptualization. **Haiyue Zu:** Validation. **Weishi Li:** Supervision, Funding acquisition, Conceptualization. **Yufeng Zheng:** Writing – review & editing, Visualization, Validation, Supervision, Conceptualization.

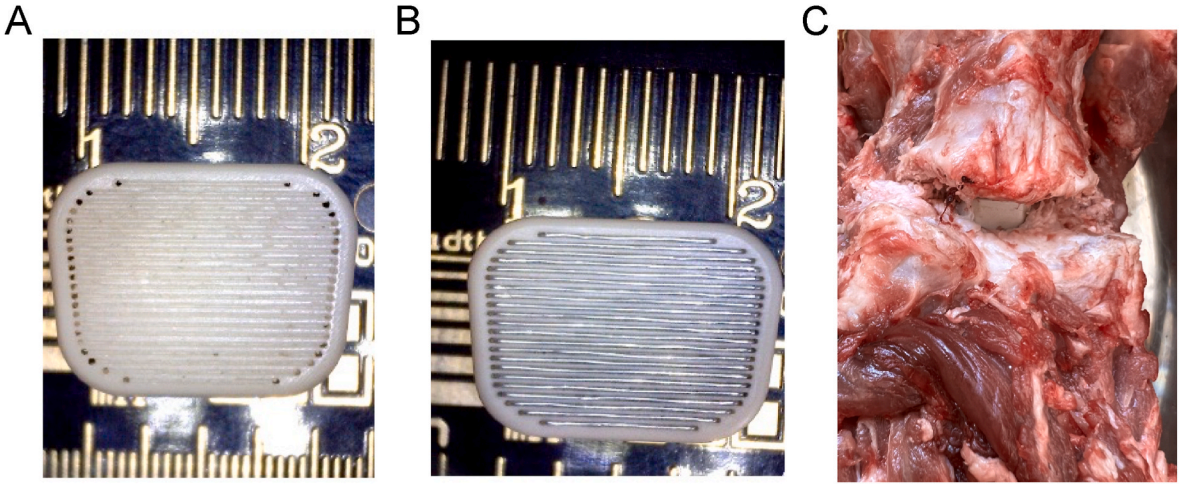

Fig. 10. The first generation of Mg-PEEK spine fusion cage, A. PEEK-based cage with processed embedding canals; B. PEEK-based cage embedding with Mg wire; C. the goat cadaver test for Mg-PEEK cage.

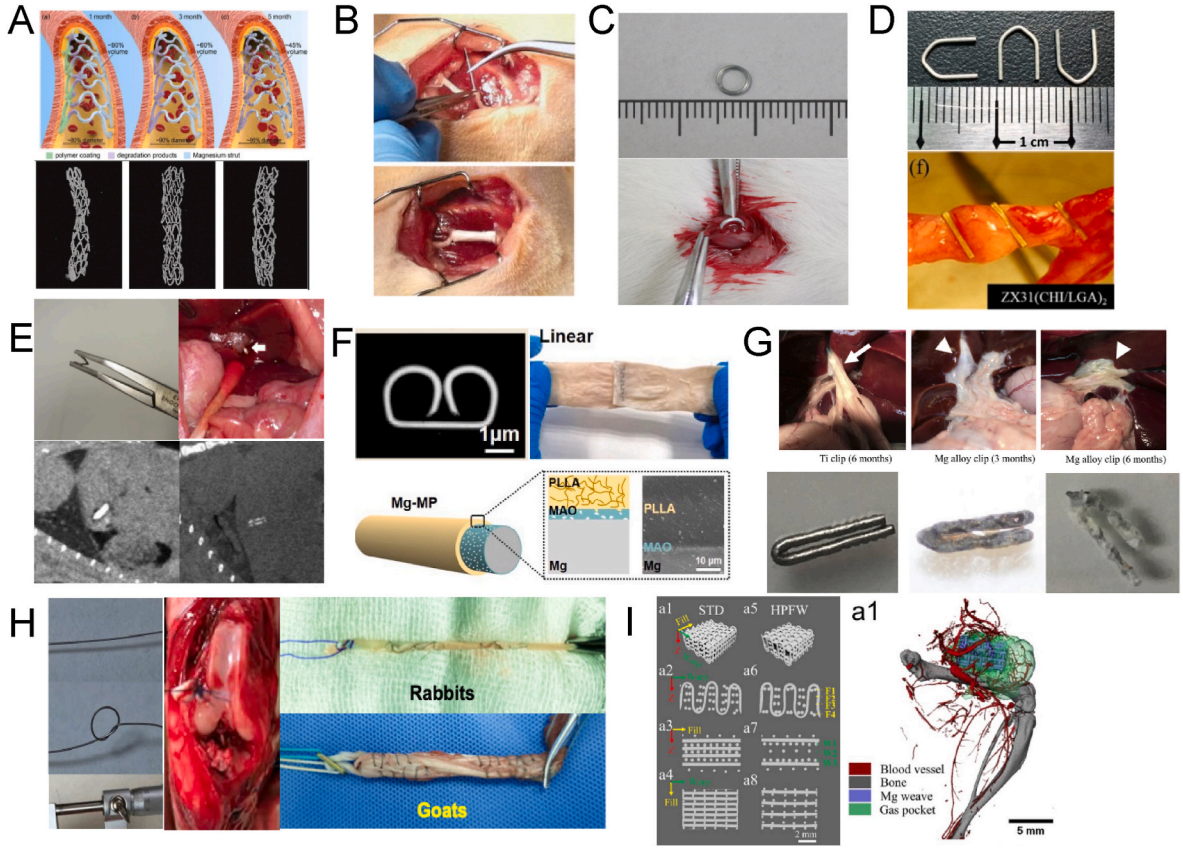

Fig. 11. A. Mg based coronary artery stent, Zong et al. [276], copyright 2022, ELSVIER, Creative Commons Attribution License; B. Mg wire induced nerve regeneration, Vennemeyer et al. [280], copyright 2015, SAGE; C. Mg wire ligated bladder, Okamura et al. [281], copyright 2021, Springer; D. Mg wire ligated urinary tract, Chang et al. [282], copyright 2020, MDPI, Creative Commons Attribution License; E. Mg wire used for hepatectomy, Urade et al. [279], copyright 2019, BMC, Creative Commons Attribution 4.0 International License; F. Mg wire anastomosed intestine, Zhang et al. [277], copyright 2023, Ke Ai, Creative Commons Attribution License; G. Mg wire used for cholecystectomy, Yoshida et al. [278], copyright, 2017, ELSEVIER; H. Mg wire weaving ACL tendon graft in reconstruction surgery, He et al. [62,91], copyright 2022, MDPI, Creative Commons Attribution License and 2024, Ke Ai, Creative Commons Attribution License; I. Mg based scaffold based on Mg wire to treat defect, Xue et al. [283], copyright 2022, IOP, Creative Commons Attribution License.

Declaration of competing interest

This study was supported by Beijing Municipal Science and Technology Project (Z201100005520073), Key Clinical projects of Peking University Third hospital (BYSY2022064), China Postdoctoral Science Foundation (M2023740146), and National Natural Science Foundation of China (82302731).

Yufeng Zheng is editor-in-chief for Bioactive Materials and was not involved in the editorial review or the decision to publish this article. All authors declare that there are no competing interests.

References

[1] N. Manam, W. Harun, D. Shri, S. Ghani, T. Kurniawan, M.H. Ismail, M. Ibrahim, Study of corrosion in biocompatible metals for implants: a review, J. Alloys Compd. 701 (2017) 698–715.
[2] G. Reith, V. Schmitz-Greven, K.O. Hensel, M.M. Schneider, T. Tinschmann, B. Bouillon, C. Probst, Metal implant removal: benefits and drawbacks–a patient survey, BMC Surg. 15 (1) (2015) 1–8.
[3] B.R. Williams, D.L. McCreary, M. Chau, B.P. Cunningham, F. Pena, M. F. Swiontkowski, Functional outcomes of symptomatic implant removal following ankle fracture open reduction and internal fixation, Foot Ankle Int. 39 (6) (2018) 674–680.
[4] S. Lovald, D. Mercer, J. Hanson, I. Cowgill, M. Erdman, P. Robinson, B. Diamond, Complications and hardware removal after open reduction and internal fixation of humeral fractures, J. Trauma 70 (5) (2011) 1273–1277. ; discussion 1277-8.
[5] P.J. Ostergaard, M.J. Hall, G. Xiong, D. Zhang, B.E. Earp, Risk factors for implant removal after surgical fixation of midshaft clavicle fractures, Orthopedics 45 (4) (2022) e201–e206.
[6] P.T. Liu, W.P. Pavlicek, M.B. Peter, M.J. Spangehl, C.C. Roberts, R.G. Paden, Metal artifact reduction image reconstruction algorithm for CT of implanted metal orthopedic devices: a work in progress, Skeletal Radiol. 38 (8) (2009) 797–802.
[7] B.D. Ulery, L.S. Nair, C.T. Laurencin, Biomedical applications of biodegradable polymers, J. Polym. Sci., Part B: Polym. Phys. 49 (12) (2011) 832–864.
[8] R. Song, M. Murphy, C. Li, K. Ting, C. Soo, Z. Zheng, Current development of biodegradable polymeric materials for biomedical applications, Drug Des. Dev. Ther. 12 (2018) 3117.
[9] S. Farah, D.G. Anderson, R. Langer, Physical and mechanical properties of PLA, and their functions in widespread applications—a comprehensive review, Adv. Drug Deliv. Rev. 107 (2016) 367–392.
[10] S. Bose, D. Banerjee, A. Bandyopadhyay, Introduction to Biomaterials and Devices for Bone Disorders, Materials for Bone Disorders, Elsevier, 2017, pp. 1–27.
[11] S. Seaman, P. Kerezoudis, M. Bydon, J.C. Torner, P.W. Hitchon, Titanium vs. polyetheretherketone (PEEK) interbody fusion: meta-analysis and review of the literature, J. Clin. Neurosci. : official journal of the Neurosurgical Society of Australasia 44 (2017) 23–29.
[12] N. Saris, E. Mervaala, H. Karppanen, J. Khawaja, A. Lewenstam, 891 Magnesium. An update onphysiological, clinical and analytical aspects, Clin 892 Chim Acta 294 (1–26) (2000) 893.
[13] H. Rubin, Central roles of Mg2+ and MgATP2− in the regulation of protein synthesis and cell proliferation: significance for neoplastic transformation, Adv. Cancer Res. 93 (2005) 1–58.
[14] F. Witte, Reprint of: the history of biodegradable magnesium implants: a review, Acta Biomater. 23 (2015) S28–S40.
[15] R. Zeng, W. Dietzel, F. Witte, N. Hort, C. Blawert, Progress and challenge for magnesium alloys as biomaterials, Adv. Eng. Mater. 10 (8) (2008) B3–B14.
[16] H. Zu, K. Chau, T.O. Olugbade, L. Pan, C.H. Dreyer, H.K. Chow, L. Huang, L. Zheng, W. Tong, X. Li, Comparison of modified injection molding and conventional machining in biodegradable behavior of perforated cannulated magnesium hip stents, J. Mater. Sci. Technol. (2021).
[17] G. Wu, K.-C. Chan, L. Zhu, L. Sun, J. Lu, Dual-phase nanostructuring as a route to high-strength magnesium alloys, Nature 545 (7652) (2017) 80–83.
[18] X. Yan, X. Meng, L. Luo, Y. Jing, G. Yi, J. Lu, Y. Liu, Mechanical behaviour of AZ31 magnesium alloy with the laminate and gradient structure, Phil. Mag. 99 (24) (2019) 3059–3077.

[19] J.Y. Rho, L. Kuhn-Spearing, P. Zioupos, Mechanical properties and the hierarchical structure of bone, Med. Eng. Phys. 20 (2) (1998) 92–102.
[20] F. Witte, N. Hort, C. Vogt, S. Cohen, F. Feyerabend, Degradable biomaterials based on magnesium corrosion, Curr. Opin. Solid State Mater. Sci. 12 (5) (2008) 63–72.
[21] G.E.J. Poinern, S. Brundavanam, D. Fawcett, Biomedical Magnesium Alloys: A Review of Material Properties, Surface Modifications and Potential as a Biodegradable Orthopaedic Implant, american journal of biomedical engineering, 2012.
[22] Q. Peng, X. Li, M. Ning, R. Liu, H. Zhang, Effects of backward extrusion on mechanical and degradation properties of Mg-Zn biomaterial, J. Mech. Behav. Biomed. Mater. 10 (none) (2012) 128–137.
[23] B. Zhang, Y. Hou, X. Wang, W. Yin, G. Lin, Mechanical properties, degradation performance and cytotoxicity of Mg–Zn–Ca biomedical alloys with different compositions, Mater. Sci. Eng. C 31 (8) (2011) 1667–1673.
[24] P.C. Gautam, S. Biswas, On the possibility to reduce ECAP deformation temperature in magnesium: deformation behaviour, dynamic recrystallization and mechanical properties, Mater. Sci. Eng., A 812 (2021) 141103.
[25] Q. Wu, S. Zhu, L. Wang, Q. Liu, S. Guan, The microstructure and properties of cyclic extrusion compression treated Mg-Zn-Y-Nd alloy for vascular stent application, J. Mech. Behav. Biomed. Mater. 8 (2) (2012) 1–7.
[26] X. Zhao, L.-l. Shi, J. Xu, Biodegradable Mg–Zn–Y alloys with long-period stacking ordered structure: optimization for mechanical properties, J. Mech. Behav. Biomed. Mater. 18 (2013) 181–190.
[27] J. Chen, L. Tan, I.P. Etim, K. Yang, Comparative study of the effect of Nd and Y content on the mechanical and biodegradable properties of Mg-Zn-Zr-xNd/Y (x= 0.5, 1, 2) alloys, Mater. Technol. 33 (10) (2018) 659–671.
[28] Y. Yang, J. Guo, C. Wang, T. Zhang, W. Jiang, Z. Zhang, Q. Wang, G. Li, J. Wang, The effects of deformation parameters and cooling rates on the aging behavior of AZ80+ 0.4% Ce, J. Magnesium Alloys (2022).
[29] H. Miao, D. Zhang, C. Chen, L. Zhang, J. Pei, Y. Su, H. Huang, Z. Wang, B. Kang, W. Ding, Research on biodegradable Mg–Zn–Gd alloys for potential orthopedic implants: in vitro and in vivo evaluations, ACS Biomater. Sci. Eng. 5 (3) (2019) 1623–1634.
[30] Q. Chen, Z. Zhao, Z. Zhao, C. Hu, D. Shu, Microstructure development and thixoextrusion of magnesium alloy prepared by repetitive upsetting-extrusion, J. Alloys Compd. 509 (26) (2011) 7303–7315.
[31] Y.C. Li, M.H. Li, W.Y. Hu, P.D. Hodgson, C.E. Wen, Biodegradable Mg-Ca and Mg-Ca-Y alloys for regenerative medicine, Mater. Sci. Forum (2010) 2192–2195.
[32] I.S. Berglund, E.W. Dirr, V. Ramaswamy, J.B. Allen, K.D. Allen, The effect of Mg–Ca–Sr alloy degradation products on human mesenchymal stem cells, J. Biomed. Mater. Res. B Appl. Biomater. 106 (2) (2018) 697–704.
[33] F. Kiani, J. Lin, A. Vahid, K. Munir, C. Wen, Y. Li, Microstructures, mechanical properties, corrosion, and biocompatibility of extruded Mg-Zr-Sr-Ho alloys for biodegradable implant applications, J. Magnesium Alloys 11 (1) (2023) 110–136.
[34] X. Gu, X. Xie, N. Li, Y. Zheng, L. Qin, In vitro and in vivo studies on a Mg–Sr binary alloy system developed as a new kind of biodegradable metal, Acta Biomater. 8 (6) (2012) 2360–2374.
[35] M. Hu, H. Fei, J. Gao, F.F. Zhao, A study on microstructures and creep behaviors in the Mg-3Sr-xY alloys, Adv. Mater. Res. 418–420 (2011) 602–605.
[36] A. Kula, X. Jia, R. Mishra, M. Niewczas, Flow stress and work hardening of Mg-Y alloys, Int. J. Plast. 92 (2017) 96–121.
[37] D.T. Chou, D. Hong, P. Saha, J. Ferrero, B. Lee, Z. Tan, Z. Dong, P.N. Kumta, In vitro and in vivo corrosion, cytocompatibility and mechanical properties of biodegradable Mg–Y–Ca–Zr alloys as implant materials, Acta Biomater. 9 (10) (2013) 8518–8533.
[38] I. Stulikova, B. Smola, Mechanical properties and phase composition of potential biodegradable Mg–Zn–Mn–base alloys with addition of rare earth elements, Mater. Char. 61 (10) (2010) 952–958.
[39] Q. Peng, H. Fu, J. Pang, J. Zhang, W. Xiao, Preparation, Mechanical and Degradation Properties of Mg–Y-Based Microwire, 2013.
[40] G. Liu, J. Zhang, G. Xi, R. Zuo, S. Liu, Designing Mg alloys with high ductility: reducing the strength discrepancies between soft deformation modes and hard deformation modes, Acta Mater. 141 (2017) 1–9.
[41] X. Zhang, G. Yuan, L. Mao, J. Niu, P. Fu, W. Ding, Effects of extrusion and heat treatment on the mechanical properties and biocorrosion behaviors of a Mg–Nd–Zn–Zr alloy, J. Mech. Behav. Biomed. Mater. 7 (2012) 77–86.
[42] R. Sabat, A. Brahme, R. Mishra, K. Inal, S. Suwas, Ductility enhancement in Mg-0.2% Ce alloys, Acta Mater. 161 (2018) 246–257.
[43] R. Sabat, R. Mishra, A. Sachdev, S. Suwas, The deciding role of texture on ductility in a Ce containing Mg alloy, Mater. Lett. 153 (2015) 158–161.
[44] P. Hidalgo-Manrique, J. Robson, M. Pérez-Prado, Precipitation strengthening and reversed yield stress asymmetry in Mg alloys containing rare-earth elements: a quantitative study, Acta Mater. 124 (2017) 456–467.
[45] S. Sandlöbes, Z. Pei, M. Friák, L.-F. Zhu, F. Wang, S. Zaefferer, D. Raabe, J. Neugebauer, Ductility improvement of Mg alloys by solid solution: ab initio modeling, synthesis and mechanical properties, Acta Mater. 70 (2014) 92–104.
[46] A. Luo, C. Zhang, A. Sachdev, Effect of eutectic temperature on the extrudability of magnesium–aluminum alloys, Scripta Mater. 66 (7) (2012) 491–494.
[47] J.-Y. Lee, Y.-S. Yun, B.-C. Suh, N.-J. Kim, W.-T. Kim, D.-H. Kim, Comparison of static recrystallization behavior in hot rolled Mg–3Al–1Zn and Mg–3Zn–0.5 Ca sheets, J. Alloys Compd. 589 (2014) 240–246.
[48] T. Zhou, Z. Yang, D. Hu, T. Feng, M. Yang, X. Zhai, Effect of the final rolling speeds on the stretch formability of AZ31 alloy sheet rolled at a high temperature, J. Alloys Compd. 650 (2015) 436–443.
[49] X. Huang, K. Suzuki, Y. Chino, M. Mabuchi, Texture and stretch formability of AZ61 and AM60 magnesium alloy sheets processed by high-temperature rolling, J. Alloys Compd. 632 (2015) 94–102.
[50] X. Huang, K. Suzuki, Y. Chino, M. Mabuchi, Influence of aluminum content on the texture and sheet formability of AM series magnesium alloys, Mater. Sci. Eng., A 633 (2015) 144–153.
[51] Y. Chino, M. Mabuchi, Enhanced stretch formability of Mg–Al–Zn alloy sheets rolled at high temperature (723 K), Scripta Mater. 60 (6) (2009) 447–450.
[52] Z. Geng, D. Xiao, L. Chen, Microstructure, mechanical properties, and corrosion behavior of degradable Mg-Al-Cu-Zn-Gd alloys, J. Alloys Compd. 686 (2016) 145–152.
[53] T.-C. Chang, J.-Y. Wang, C.-L. Chu, S. Lee, Mechanical properties and microstructures of various Mg–Li alloys, Mater. Lett. 60 (27) (2006) 3272–3276.
[54] C. Krause, D. Bormann, T. Hassel, F.W. Bach, A. Krause, Mechanical Properties of Degradable Magnesium Implants in Dependence of the Implantation Duration, 2006.
[55] D. Zhao, F. Witte, F. Lu, J. Wang, J. Li, L. Qin, Current status on clinical applications of magnesium-based orthopaedic implants: a review from clinical translational perspective, Biomaterials 112 (2017) 287–302.
[56] X.N. Gu, X.H. Xie, N. Li, Y.F. Zheng, L. Qin, In vitro and in vivo studies on a Mg-Sr binary alloy system developed as a new kind of biodegradable metal, Acta Biomater. 8 (6) (2012) 2360–2374.
[57] P. Scheltens, B. De Strooper, M. Kivipelto, H. Holstege, G. Chételat, C. E. Teunissen, J. Cummings, W.M. van der Flier, Alzheimer's disease, Lancet (London, England) 397 (10284) (2021) 1577–1590.
[58] M. Esmaily, J. Svensson, S. Fajardo, N. Birbilis, G. Frankel, S. Virtanen, R. Arrabal, S. Thomas, L. Johansson, Fundamentals and advances in magnesium alloy corrosion, Prog. Mater. Sci. 89 (2017) 92–193.
[59] X. Zhang, G. Yuan, J. Niu, P. Fu, W. Ding, Microstructure, mechanical properties, biocorrosion behavior, and cytotoxicity of as-extruded Mg–Nd–Zn–Zr alloy with different extrusion ratios, J. Mech. Behav. Biomed. Mater. 9 (none) (2012) 153–162.
[60] J. Gonzalez, R.Q. Hou, E.P. Nidadavolu, R. Willumeit-Römer, F. Feyerabend, Magnesium degradation under physiological conditions–Best practice, Bioact. Mater. 3 (2) (2018) 174–185.
[61] M. Pogorielov, E. Husak, A. Solodivnik, S. Zhdanov, Magnesium-based biodegradable alloys: degradation, application, and alloying elements, Interventional Medicine and Applied Science 9 (1) (2017) 27–38.
[62] X. He, Y. Li, H. Miao, J. Xu, M.T.-y. Ong, C. Wang, L. Zheng, J. Wang, L. Huang, H. Zu, High formability Mg-Zn-Gd wire facilitates ACL reconstruction via its swift degradation to accelerate intra-tunnel endochondral ossification, J. Magnesium Alloys (2022).
[63] J.W. Lee, H.S. Han, K.J. Han, J. Park, H. Jeon, M.R. Ok, H.K. Seok, J.P. Ahn, K. E. Lee, D.H. Lee, S.J. Yang, S.Y. Cho, P.R. Cha, H. Kwon, T.H. Nam, J.H. Han, H. J. Rho, K.S. Lee, Y.C. Kim, D. Mantovani, Long-term clinical study and multiscale analysis of in vivo biodegradation mechanism of Mg alloy, Proc. Natl. Acad. Sci. U.S.A. 113 (3) (2016) 716–721.
[64] D. Krüger, S. Galli, B. Zeller-Plumhoff, D.F. Wieland, N. Peruzzi, B. Wiese, P. Heuser, J. Moosmann, A. Wennerberg, R. Willumeit-Römer, High-resolution ex vivo analysis of the degradation and osseointegration of Mg-xGd implant screws in 3D, Bioact. Mater. 13 (2022) 37–52.
[65] J. Kuhlmann, I. Bartsch, E. Willbold, S. Schuchardt, O. Holz, N. Hort, D. Höche, W.R. Heineman, F. Witte, Fast escape of hydrogen from gas cavities around corroding magnesium implants, Acta Biomater. 9 (10) (2013) 8714–8721.
[66] G. Song, A. Atrens, Understanding magnesium corrosion—a framework for improved alloy performance, Adv. Eng. Mater. 5 (12) (2003) 837–858.
[67] G. Song, Control of biodegradation of biocompatable magnesium alloys, Corrosion Sci. 49 (4) (2007) 1696–1701.
[68] Z. Qiao, Z. Shi, N. Hort, N.I.Z. Abidin, A. Atrens, Corrosion behaviour of a nominally high purity Mg ingot produced by permanent mould direct chill casting, Corrosion Sci. 61 (2012) 185–207.
[69] S.E. Henderson, K. Verdelis, S. Maiti, S. Pal, W.L. Chung, D.-T. Chou, P.N. Kumta, A.J. Almarza, Magnesium alloys as a biomaterial for degradable craniofacial screws, Acta Biomater. 10 (5) (2014) 2323–2332.
[70] P. Makkar, S.K. Sarkar, A.R. Padalhin, B.-G. Moon, Y.S. Lee, B.T. Lee, In vitro and in vivo assessment of biomedical Mg–Ca alloys for bone implant applications, J. Appl. Biomater. Funct. Mater. 16 (3) (2018) 126–136.
[71] Y. Hu, X. Guo, Y. Qiao, X. Wang, Q. Lin, Preparation of medical Mg–Zn alloys and the effect of different zinc contents on the alloy, J. Mater. Sci. Mater. Med. 33 (1) (2022) 9.
[72] D.N. Pham, S. Hiromoto, T. Yamazaki, M. O, E. Kobayashi, Enhanced corrosion resistance and in vitro biocompatibility of Mg-Zn alloys by carbonate apatite coating, ACS Appl. Bio Mater. 4 (9) (2021) 6881–6892.
[73] M. Grimm, A. Lohmüller, R.F. Singer, S. Virtanen, Influence of the microstructure on the corrosion behaviour of cast Mg-Al alloys, Corrosion Sci. 155 (2019) 195–208.
[74] G.E.J. Poinern, S. Brundavanam, D. Fawcett, Biomedical magnesium alloys: a review of material properties, surface modifications and potential as a biodegradable orthopaedic implant, Am. J. Biomed. Eng. 2 (6) (2012) 218–240.
[75] R. Kumar, P. Katyal, Effects of alloying elements on performance of biodegradable magnesium alloy, Mater. Today: Proc. 56 (2022) 2443–2450.
[76] W. Zhang, M. Li, Q. Chen, W. Hu, W. Zhang, W. Xin, Effects of Sr and Sn on microstructure and corrosion resistance of Mg–Zr–Ca magnesium alloy for biomedical applications, Mater. Des. 39 (2012) 379–383.
[77] F. Sayari, R. Mahmudi, R. Roumina, Inducing superplasticity in extruded pure Mg by Zr addition, Mater. Sci. Eng., A 769 (2020) 138502.

[78] S. Suliman, H.J. Aljudy, Effect of niobium nitride coating by magnetron sputtering on corrosion resistance of biodegradable magnesium-Strontium alloy, Pak. J. Med. Health Sci 15 (2021) 348–353.
[79] W. Jiang, A.F. Cipriano, Q. Tian, C. Zhang, M. Lopez, A. Sallee, A. Lin, M.C. C. Alcaraz, Y. Wu, Y. Zheng, In vitro evaluation of MgSr and MgCaSr alloys via direct culture with bone marrow derived mesenchymal stem cells, Acta Biomater. 72 (2018) 407–423.
[80] O. Pavlic, W. Ibarra-Hernandez, I. Valencia-Jaime, S. Singh, G. Avendaño-Franco, D. Raabe, A.H. Romero, Design of Mg alloys: the effects of Li concentration on the structure and elastic properties in the Mg-Li binary system by first principles calculations, J. Alloys Compd. 691 (2017) 15–25.
[81] K. Kumar, R. Gill, U. Batra, Challenges and opportunities for biodegradable magnesium alloy implants, Mater. Technol. 33 (2) (2018) 153–172.
[82] Q. Luo, Y. Guo, B. Liu, Y. Feng, J. Zhang, Q. Li, K. Chou, Thermodynamics and kinetics of phase transformation in rare earth–magnesium alloys: a critical review, J. Mater. Sci. Technol. 44 (2020) 171–190.
[83] H. Azzeddine, A. Hanna, A. Dakhouche, L. Rabahi, N. Scharnagl, M. Dopita, F. Brisset, A.-L. Helbert, T. Baudin, Impact of rare-earth elements on the corrosion performance of binary magnesium alloys, J. Alloys Compd. 829 (2020) 154569.
[84] A.H.M. Sanchez, B.J. Luthringer, F. Feyerabend, R. Willumeit, Mg and Mg alloys: how comparable are in vitro and in vivo corrosion rates? A review, Acta Biomater. 13 (2015) 16–31.
[85] W. Yan, Y.-J. Lian, Z.-Y. Zhang, M.-Q. Zeng, Z.-Q. Zhang, Z.-Z. Yin, L.-Y. Cui, R.-C. Zeng, In vitro degradation of pure magnesium—the synergetic influences of glucose and albumin, Bioact. Mater. 5 (2) (2020) 318–333.
[86] J. Walker, S. Shadanbaz, N.T. Kirkland, E. Stace, T. Woodfield, M.P. Staiger, G. J. Dias, Magnesium alloys: predicting in vivo corrosion with in vitro immersion testing, J. Biomed. Mater. Res. B Appl. Biomater. 100 (4) (2012) 1134–1141.
[87] X. Gu, Y. Zheng, Y. Cheng, S. Zhong, T. Xi, In vitro corrosion and biocompatibility of binary magnesium alloys, Biomaterials 30 (4) (2009) 484–498.
[88] N.I.Z. Abidin, B. Rolfe, H. Owen, J. Malisano, D. Martin, J. Hofstetter, P. J. Uggowitzer, A. Atrens, The in vivo and in vitro corrosion of high-purity magnesium and magnesium alloys WZ21 and AZ91, Corrosion Sci. 75 (2013) 354–366.
[89] N. Kirkland, N. Birbilis, M. Staiger, Assessing the corrosion of biodegradable magnesium implants: a critical review of current methodologies and their limitations, Acta Biomater. 8 (3) (2012) 925–936.
[90] W.D. Mueller, M. Fernandez Lorenzo de Mele, M.L. Nascimento, M. Zeddies, Degradation of magnesium and its alloys: dependence on the composition of the synthetic biological media, J. Biomed. Mater. Res. Part A: An Official Journal of The Society for Biomaterials, The Japanese Society for Biomaterials, and The Australian Society for Biomaterials and the Korean Society for Biomaterials 90 (2) (2009) 487–495.
[91] X. He, Y. Li, H. Miao, J. Sun, M.T.Y. Ong, H. Zu, W. Li, The bioactive Mg-Zn-Gd wire enhances musculoskeletal regeneration: an in vitro study, Crystals 12 (9) (2022) 1287.
[92] F. Feyerabend, H. Drücker, D. Laipple, C. Vogt, M. Stekker, N. Hort, R. Willumeit, Ion release from magnesium materials in physiological solutions under different oxygen tensions, J. Mater. Sci. Mater. Med. 23 (1) (2012) 9–24.
[93] R.-Q. Hou, N. Scharnagl, R. Willumeit-Römer, F. Feyerabend, Different effects of single protein vs. protein mixtures on magnesium degradation under cell culture conditions, Acta Biomater. 98 (2019) 256–268.
[94] D.A. Bushinsky, Metabolic alkalosis decreases bone calcium efflux by suppressing osteoclasts and stimulating osteoblasts, Am. J. Physiol. Ren. Physiol. 271 (1) (1996) F216–F222.
[95] A.-M. Galow, A. Rebl, D. Koczan, S.M. Bonk, W. Baumann, J. Gimsa, Increased osteoblast viability at alkaline pH in vitro provides a new perspective on bone regeneration, Biochemistry and biophysics reports 10 (2017) 17–25.
[96] J.-W. Kim, A.M.D. Alfafara, H.-Y. Kim, S.-Y. Kim, S.-J. Kim, Effects of pH alteration on the pathogenesis of medication-related osteonecrosis of the jaw, Bone 122 (2019) 45–51.
[97] Z. Shi, M. Liu, A. Atrens, Measurement of the corrosion rate of magnesium alloys using Tafel extrapolation, Corrosion Sci. 52 (2) (2010) 579–588.
[98] J.M. Seitz, K. Collier, E. Wulf, D. Bormann, F.W. Bach, Comparison of the corrosion behavior of coated and uncoated magnesium alloys in an in vitro corrosion environment, Adv. Eng. Mater. 13 (9) (2011) B313–B323.
[99] Z. Zhen, T.-f. Xi, Y.-f. Zheng, A review on in vitro corrosion performance test of biodegradable metallic materials, Trans. Nonferrous Metals Soc. China 23 (8) (2013) 2283–2293.
[100] F. Witte, J. Fischer, J. Nellesen, H.-A. Crostack, V. Kaese, A. Pisch, F. Beckmann, H. Windhagen, In vitro and in vivo corrosion measurements of magnesium alloys, Biomaterials 27 (7) (2006) 1013–1018.
[101] H.M. Wong, K.W. Yeung, K.O. Lam, V. Tam, P.K. Chu, K.D. Luk, K.M. Cheung, A biodegradable polymer-based coating to control the performance of magnesium alloy orthopaedic implants, Biomaterials 31 (8) (2010) 2084–2096.
[102] J. Wang, Y. Wu, H. Li, Y. Liu, X. Bai, W. Chau, Y. Zheng, L. Qin, Magnesium alloy based interference screw developed for ACL reconstruction attenuates peri-tunnel bone loss in rabbits, Biomaterials 157 (2018) 86–97.
[103] W.A. Badawy, N.H. Hilal, M. El-Rabiee, H. Nady, Electrochemical behavior of Mg and some Mg alloys in aqueous solutions of different pH, Electrochim. Acta 55 (6) (2010) 1880–1887.
[104] F. Witte, V. Kaese, H. Haferkamp, E. Switzer, A. Meyer-Lindenberg, C. Wirth, H. Windhagen, In vivo corrosion of four magnesium alloys and the associated bone response, Biomaterials 26 (17) (2005) 3557–3563.
[105] N. Erdmann, A. Bondarenko, M. Hewicker-Trautwein, N. Angrisani, J. Reifenrath, A. Lucas, A. Meyer-Lindenberg, Evaluation of the soft tissue biocompatibility of MgCa0. 8 and surgical steel 316L in vivo: a comparative study in rabbits, Biomed. Eng. Online 9 (1) (2010) 1–17.
[106] H. Xuan, L. Ye, G. Jiaxin, X. Jiankun, Z. Haiyue, L. Huang, Q. Ling, Biomaterials developed for facilitating healing outcome after anterior cruciate ligament reconstruction: efficacy, surgical protocols, and assessments using preclinical animal models, Biomaterials (2020) 120625.
[107] S. Sefa, D. Wieland, H. Helmholz, B. Zeller-Plumhoff, A. Wennerberg, J. Moosmann, R. Willumeit-Römer, S. Galli, Assessing the long-term in vivo degradation behavior of magnesium alloys-a high resolution synchrotron radiation micro computed tomography study, Frontiers in Biomaterials Science 1 (2022) 925471.
[108] R.F. Wallin, E. Arscott, A Practical Guide to ISO 10993-5: Cytotoxicity, Medical Device and Diagnostic Industry, 20, 1998, pp. 96–98.
[109] Z. Zhen, X. Liu, T. Huang, T. Xi, Y. Zheng, Hemolysis and cytotoxicity mechanisms of biodegradable magnesium and its alloys, Mater. Sci. Eng. C 46 (2015) 202–206.
[110] J. Durlach, V. Durlach, P. Bac, M. Bara, A. Guiet-Bara, Magnesium and therapeutics, Magnes. Res. 7 (3–4) (1994) 313–328.
[111] K.-J. Kim, S. Choi, Y.S. Cho, S.-J. Yang, Y.-S. Cho, K.K. Kim, Magnesium ions enhance infiltration of osteoblasts in scaffolds via increasing cell motility, J. Mater. Sci. Mater. Med. 28 (6) (2017) 96.
[112] Z. Yao, W. Yuan, J. Xu, W. Tong, J. Mi, P.C. Ho, D.H.K. Chow, Y. Li, H. Yao, X. Li, Magnesium-encapsulated injectable hydrogel and 3D-engineered polycaprolactone conduit facilitate peripheral nerve regeneration, Adv. Sci. (2022) 2202102.
[113] Y. Li, J. Xu, J. Mi, X. He, Q. Pan, L. Zheng, H. Zu, Z. Chen, B. Dai, X. Li, Biodegradable magnesium combined with distraction osteogenesis synergistically stimulates bone tissue regeneration via CGRP-FAK-VEGF signaling axis, Biomaterials (2021) 120984.
[114] J. Wang, F. Witte, T. Xi, Y. Zheng, K. Yang, Y. Yang, D. Zhao, J. Meng, Y. Li, W. Li, Recommendation for modifying current cytotoxicity testing standards for biodegradable magnesium-based materials, Acta Biomater. 21 (2015) 237–249.
[115] S. Zhang, X. Zhang, C. Zhao, J. Li, Y. Song, C. Xie, H. Tao, Y. Zhang, Y. He, Y. Jiang, Research on an Mg–Zn alloy as a degradable biomaterial, Acta Biomater. 6 (2) (2010) 626–640.
[116] A. Mehjabeen, T. Song, W. Xu, H.P. Tang, M. Qian, Zirconium alloys for orthopaedic and dental applications, Adv. Eng. Mater. 20 (9) (2018) 1800207.
[117] M. Kim, S. An, C. Huh, C. Kim, Development of zirconium-based alloys with low elastic modulus for dental implant materials, Appl. Sci. 9 (24) (2019) 5281.
[118] E. Inan-Eroglu, A. Ayaz, Is aluminum exposure a risk factor for neurological disorders?, in: Journal of Research in Medical Sciences, 23 The official journal of Isfahan University of Medical Sciences, 2018.
[119] A. Loos, R. Rohde, A. Haverich, S. Barlach, In Vitro and in Vivo Biocompatibility Testing of Absorbable Metal Stents, Wiley Online Library, Macromolecular Symposia, 2007, pp. 103–108.
[120] M. Kawagoe, F. Hirasawa, S.C. Wang, Y. Liu, Y. Ueno, T. Sugiyama, Orally administrated rare earth element cerium induces metallothionein synthesis and increases glutathione in the mouse liver, Life Sci. 77 (8) (2005) 922–937.
[121] N. Murata, K. Murata, L.F. Gonzalez-Cuyar, K.R. Maravilla, Gadolinium tissue deposition in brain and bone, Magn. Reson. Imag. 34 (10) (2016) 1359–1365.
[122] T.H. Darrah, J.J. Prutsman-Pfeiffer, R.J. Poreda, M. Ellen Campbell, P. V. Hauschka, R.E. Hannigan, Incorporation of excess gadolinium into human bone from medical contrast agents, Metallomics 1 (6) (2009) 479–488.
[123] D. Noviana, D. Paramitha, M.F. Ulum, H. Hermawan, The effect of hydrogen gas evolution of magnesium implant on the postimplantation mortality of rats, Journal of Orthopaedic Translation 5 (2016) 9–15.
[124] K.-i. Fukuda, S. Asoh, M. Ishikawa, Y. Yamamoto, I. Ohsawa, S. Ohta, Inhalation of hydrogen gas suppresses hepatic injury caused by ischemia/reperfusion through reducing oxidative stress, Biochem. Biophys. Res. Commun. 361 (3) (2007) 670–674.
[125] I. Ohsawa, M. Ishikawa, K. Takahashi, M. Watanabe, K. Nishimaki, K. Yamagata, K.-i. Katsura, Y. Katayama, S. Asoh, S. Ohta, Hydrogen acts as a therapeutic antioxidant by selectively reducing cytotoxic oxygen radicals, Nat. Med. 13 (6) (2007) 688–694.
[126] C.M. Muth, E.S. Shank, Gas embolism, N. Engl. J. Med. 342 (7) (2000) 476–482.
[127] R.A. van Hulst, J. Klein, B. Lachmann, Gas embolism: pathophysiology and treatment, Clin. Physiol. Funct. Imag. 23 (5) (2003) 237–246.
[128] E. McBride, Magnesium screw and nail transfixion in fractures, South. Med. J. 31 (5) (1938) 508–514.
[129] Witte Frank, The history of biodegradable magnesium implants: a review, Acta Biomater. (2010).
[130] M. Rahman, N.K. Dutta, N. Roy Choudhury, Magnesium alloys with tunable interfaces as bone implant materials, Front. Bioeng. Biotechnol. 8 (2020) 564.
[131] U.C. Nwaogu, C. Blawert, N. Scharnagl, W. Dietzel, K. Kainer, Effects of organic acid pickling on the corrosion resistance of magnesium alloy AZ31 sheet, Corrosion Sci. 52 (6) (2010) 2143–2154.
[132] U.C. Nwaogu, C. Blawert, N. Scharnagl, W. Dietzel, K. Kainer, Influence of inorganic acid pickling on the corrosion resistance of magnesium alloy AZ31 sheet, Corrosion Sci. 51 (11) (2009) 2544–2556.
[133] M.C. Turhan, R. Lynch, M.S. Killian, S. Virtanen, Effect of acidic etching and fluoride treatment on corrosion performance in Mg alloy AZ91D (MgAlZn), Electrochim. Acta 55 (1) (2009) 250–257.
[134] J. Gray, B. Luan, Protective coatings on magnesium and its alloys—a critical review, J. Alloys Compd. 336 (1–2) (2002) 88–113.
[135] R. Supplit, T. Koch, U. Schubert, Evaluation of the anti-corrosive effect of acid pickling and sol–gel coating on magnesium AZ31 alloy, Corrosion Sci. 49 (7) (2007) 3015–3023.

[136] M.M. Gawlik, B. Wiese, A. Welle, J. González, V. Desharnais, J. Harmuth, T. Ebel, R. Willumeit-Römer, Acetic acid etching of Mg-xGd alloys, Metals 9 (2) (2019) 117.
[137] C. Lorenz, J.G. Brunner, P. Kollmannsberger, L. Jaafar, B. Fabry, S. Virtanen, Effect of surface pre-treatments on biocompatibility of magnesium, Acta Biomater. 5 (7) (2009) 2783–2789.
[138] X. Gu, W. Zheng, Y. Cheng, Y. Zheng, A study on alkaline heat treated Mg–Ca alloy for the control of the biocorrosion rate, Acta Biomater. 5 (7) (2009) 2790–2799.
[139] M. Staesche, Über die chemische Erzeugung einer dickeren magnesiumfluorid-schutzschicht auf magnesium-legierungen, Arch. Metall. 3 (1948) 99–102.
[140] M. Carboneras, M. García-Alonso, M. Escudero, Biodegradation kinetics of modified magnesium-based materials in cell culture medium, Corrosion Sci. 53 (4) (2011) 1433–1439.
[141] T. Yan, L. Tan, B. Zhang, K. Yang, Fluoride conversion coating on biodegradable AZ31B magnesium alloy, J. Mater. Sci. Technol. 30 (7) (2014) 666–674.
[142] M. Tsunoda, Y. Aizawa, K. Nakano, Y. Liu, T. Horiuchi, K. Itai, H. Tsunoda, Changes in fluoride levels in the liver, kidney, and brain and in neurotransmitters of mice after subacute administration of fluoride, Fluoride 38 (4) (2005) 284–292.
[143] M.S. Kurdi, Chronic fluorosis: the disease and its anaesthetic implications, Indian J. Anaesth. 60 (3) (2016) 157–162.
[144] E. Everett, Fluoride's effects on the formation of teeth and bones, and the influence of genetics, J. Dent. Res. 90 (5) (2011) 552–560.
[145] M. Mousny, S. Omelon, L. Wise, E.T. Everett, M. Dumitriu, D.P. Holmyard, X. Banse, J.-P. Devogelaer, M.D. Grynpas, Fluoride effects on bone formation and mineralization are influenced by genetics, Bone 43 (6) (2008) 1067–1074.
[146] L. Zhao, C. Cui, Q. Wang, S. Bu, Growth characteristics and corrosion resistance of micro-arc oxidation coating on pure magnesium for biomedical applications, Corrosion Sci. 52 (7) (2010) 2228–2234.
[147] S. Hiromoto, A. Yamamoto, Control of degradation rate of bioabsorbable magnesium by anodization and steam treatment, Mater. Sci. Eng. C 30 (8) (2010) 1085–1093.
[148] X. Gu, N. Li, W. Zhou, Y. Zheng, X. Zhao, Q. Cai, L. Ruan, Corrosion resistance and surface biocompatibility of a microarc oxidation coating on a Mg–Ca alloy, Acta Biomater. 7 (4) (2011) 1880–1889.
[149] B. Gao, S. Hao, J. Zou, W. Wu, G. Tu, C. Dong, Effect of high current pulsed electron beam treatment on surface microstructure and wear and corrosion resistance of an AZ91HP magnesium alloy, Surf. Coating. Technol. 201 (14) (2007) 6297–6303.
[150] J. Wang, J. Tang, P. Zhang, Y. Li, J. Wang, Y. Lai, L. Qin, Surface modification of magnesium alloys developed for bioabsorbable orthopedic implants: a general review, J. Biomed. Mater. Res. B Appl. Biomater. 100 (6) (2012) 1691–1701.
[151] G. Wan, M. Maitz, H. Sun, P. Li, N. Huang, Corrosion properties of oxygen plasma immersion ion implantation treated magnesium, Surf. Coating. Technol. 201 (19–20) (2007) 8267–8272.
[152] X.B. Tian, C. Wei, S. Yang, R.K. Fu, P.K. Chu, Corrosion resistance improvement of magnesium alloy using nitrogen plasma ion implantation, Surf. Coating. Technol. 198 (1–3) (2005) 454–458.
[153] X. Tian, C. Wei, S. Yang, R.K. Fu, P.K. Chu, Water plasma implantation/oxidation of magnesium alloys for corrosion resistance, Nucl. Instrum. Methods Phys. Res. Sect. B Beam Interact. Mater. Atoms 242 (1–2) (2006) 300–302.
[154] C. Liu, Y. Xin, X. Tian, P.K. Chu, Corrosion behavior of AZ91 magnesium alloy treated by plasma immersion ion implantation and deposition in artificial physiological fluids, Thin Solid Films 516 (2–4) (2007) 422–427.
[155] X. Wang, X. Zeng, G. Wu, S. Yao, Y. Lai, Effects of tantalum ion implantation on the corrosion behavior of AZ31 magnesium alloys, J. Alloys Compd. 437 (1–2) (2007) 87–92.
[156] Y. Zhao, G. Wu, H. Pan, K.W. Yeung, P.K. Chu, Formation and electrochemical behavior of Al and O plasma-implanted biodegradable Mg-Y-RE alloy, Mater. Chem. Phys. 132 (1) (2012) 187–191.
[157] H.M. Wong, Y. Zhao, V. Tam, S. Wu, P.K. Chu, Y. Zheng, M.K.T. To, F.K. Leung, K. D. Luk, K.M. Cheung, In vivo stimulation of bone formation by aluminum and oxygen plasma surface-modified magnesium implants, Biomaterials 34 (38) (2013) 9863–9876.
[158] Y. Zhao, G. Wu, Q. Lu, J. Wu, R. Xu, K.W. Yeung, P.K. Chu, Improved surface corrosion resistance of WE43 magnesium alloy by dual titanium and oxygen ion implantation, Thin Solid Films 529 (2013) 407–411.
[159] Y. Zhao, M.I. Jamesh, W.K. Li, G. Wu, C. Wang, Y. Zheng, K.W. Yeung, P.K. Chu, Enhanced antimicrobial properties, cytocompatibility, and corrosion resistance of plasma-modified biodegradable magnesium alloys, Acta Biomater. 10 (1) (2014) 544–556.
[160] R. Xu, G. Wu, X. Yang, T. Hu, Q. Lu, P.K. Chu, Controllable degradation of biomedical magnesium by chromium and oxygen dual ion implantation, Mater. Lett. 65 (14) (2011) 2171–2173.
[161] R. Xu, G. Wu, X. Yang, X. Zhang, Z. Wu, G. Sun, G. Li, P.K. Chu, Corrosion behavior of chromium and oxygen plasma-modified magnesium in sulfate solution and simulated body fluid, Appl. Surf. Sci. 258 (20) (2012) 8273–8278.
[162] Y. Guan, W. Zhou, H. Zheng, Effect of laser surface melting on corrosion behaviour of AZ91D Mg alloy in simulated-modified body fluid, J. Appl. Electrochem. 39 (2009) 1457–1464.
[163] C. Padmavathi, J.S. Sundar, S. Joshi, K. Prasad Rao, Effect of pulsed Nd: YAG laser melting treatment on microstructural and corrosion behaviour of AZ91C Mg alloy, Mater. Sci. Technol. 22 (5) (2006) 583–589.
[164] M. Sealy, Y. Guo, Surface integrity and process mechanics of laser shock peening of novel biodegradable magnesium–calcium (Mg–Ca) alloy, J. Mech. Behav. Biomed. Mater. 3 (7) (2010) 488–496.
[165] J. Chen, Y. Yang, I.P. Etim, L. Tan, K. Yang, R. Misra, J. Wang, X. Su, Recent advances on development of hydroxyapatite coating on biodegradable magnesium alloys: a review, Materials 14 (19) (2021) 5550.
[166] H. Wang, S. Guan, X. Wang, C. Ren, L. Wang, In vitro degradation and mechanical integrity of Mg–Zn–Ca alloy coated with Ca-deficient hydroxyapatite by the pulse electrodeposition process, Acta Biomater. 6 (5) (2010) 1743–1748.
[167] E. Meng, S. Guan, H. Wang, L. Wang, S. Zhu, J. Hu, C. Ren, J. Gao, Y. Feng, Effect of electrodeposition modes on surface characteristics and corrosion properties of fluorine-doped hydroxyapatite coatings on Mg–Zn–Ca alloy, Appl. Surf. Sci. 257 (11) (2011) 4811–4816.
[168] B.-D. Hahn, D.-S. Park, J.-J. Choi, J. Ryu, W.-H. Yoon, J.-H. Choi, H.-E. Kim, S.-G. Kim, Aerosol deposition of hydroxyapatite–chitosan composite coatings on biodegradable magnesium alloy, Surf. Coating. Technol. 205 (8–9) (2011) 3112–3118.
[169] L.S. Nair, C.T. Laurencin, Biodegradable polymers as biomaterials, Prog. Polym. Sci. 32 (8–9) (2007) 762–798.
[170] N. Saito, N. Murakami, J. Takahashi, H. Horiuchi, H. Ota, H. Kato, T. Okada, K. Nozaki, K. Takaoka, Synthetic biodegradable polymers as drug delivery systems for bone morphogenetic proteins, Adv. Drug Deliv. Rev. 57 (7) (2005) 1037–1048.
[171] Y. Chen, Y. Song, S. Zhang, J. Li, C. Zhao, X. Zhang, Interaction between a high purity magnesium surface and PCL and PLA coatings during dynamic degradation, Biomed. Mater. 6 (2) (2011) 025005.
[172] A. Alabbasi, S. Liyanaarachchi, M.B. Kannan, Polylactic acid coating on a biodegradable magnesium alloy: an in vitro degradation study by electrochemical impedance spectroscopy, Thin Solid Films 520 (23) (2012) 6841–6844.
[173] R.-C. Zeng, W.-C. Qi, Y.-W. Song, Q.-K. He, H.-Z. Cui, E.-H. Han, In vitro degradation of MAO/PLA coating on Mg-1.21 Li-1.12 Ca-1.0 Y alloy, Front. Mater. Sci. 8 (2014) 343–353.
[174] K. Leja, G. Lewandowicz, Polymer biodegradation and biodegradable polymers-a review, Pol. J. Environ. Stud. 19 (2) (2010).
[175] A. Reed, D. Gilding, Biodegradable polymers for use in surgery—poly (glycolic)/poly (lactic acid) homo and copolymers: 2. In vitro degradation, Polymer 22 (4) (1981) 494–498.
[176] N.J. Ostrowski, B. Lee, A. Roy, M. Ramanathan, P.N. Kumta, Biodegradable poly (lactide-co-glycolide) coatings on magnesium alloys for orthopedic applications, J. Mater. Sci. Mater. Med. 24 (2013) 85–96.
[177] J.-Y. Chen, X.-B. Chen, J.-L. Li, B. Tang, N. Birbilis, X. Wang, Electrosprayed PLGA smart containers for active anti-corrosion coating on magnesium alloy AMlite, J. Mater. Chem. A 2 (16) (2014) 5738–5743.
[178] J. Degner, F. Singer, L. Cordero, A.R. Boccaccini, S. Virtanen, Electrochemical investigations of magnesium in DMEM with biodegradable polycaprolactone coating as corrosion barrier, Appl. Surf. Sci. 282 (2013) 264–270.
[179] M. Filippi, G. Born, M. Chaaban, A. Scherberich, Natural polymeric scaffolds in bone regeneration, Front. Bioeng. Biotechnol. 8 (2020) 474.
[180] A. Fekry, A. Ghoneim, M. Ameer, Electrochemical impedance spectroscopy of chitosan coated magnesium alloys in a synthetic sweat medium, Surf. Coating. Technol. 238 (2014) 126–132.
[181] X. Gu, Y. Zheng, Q. Lan, Y. Cheng, Z. Zhang, T. Xi, D. Zhang, Surface modification of an Mg-1Ca alloy to slow down its biocorrosion by chitosan, Biomed. Mater. 4 (4) (2009) 044109.
[182] M.A. Taemeh, A. Shiravandi, M.A. Korayem, H. Daemi, Fabrication challenges and trends in biomedical applications of alginate electrospun nanofibers, Carbohydr. Polym. 228 (2020) 115419.
[183] J. Sun, H. Tan, Alginate-based biomaterials for regenerative medicine applications, Materials 6 (4) (2013) 1285–1309.
[184] H. Gao, M. Zhang, J. Zhao, L. Gao, M. Li, In vitro and in vivo degradation and mechanical properties of ZEK100 magnesium alloy coated with alginate, chitosan and mechano-growth factor, Mater. Sci. Eng. C 63 (2016) 450–461.
[185] T. Heinze, Cellulose: structure and properties, Cellulose chemistry and properties: fibers, nanocelluloses and advanced materials (2016) 1–52.
[186] N. Rahimi Roshan, H. Hassannejad, A. Nouri, Corrosion and mechanical behaviour of biodegradable PLA-cellulose nanocomposite coating on AZ31 magnesium alloy, Surf. Eng. 37 (2) (2021) 236–245.
[187] P. Neacsu, A.I. Staras, S.I. Voicu, I. Ionascu, T. Soare, S. Uzun, V.D. Cojocaru, A. M. Pandele, S.M. Croitoru, F. Miculescu, Characterization and in vitro and in vivo assessment of a novel cellulose acetate-coated Mg-based alloy for orthopedic applications, Materials 10 (7) (2017) 686.
[188] J. Necas, L. Bartosikova, P. Brauner, J. Kolar, Hyaluronic acid (hyaluronan): a review, Vet. Med. 53 (8) (2008) 397–411.
[189] Y.-K. Kim, S.-Y. Kim, Y.-S. Jang, I.-S. Park, M.-H. Lee, Bio-corrosion behaviors of hyaluronic acid and cerium multi-layer films on degradable implant, Appl. Surf. Sci. 515 (2020) 146070.
[190] Y.-K. Kim, Y.-S. Jang, S.-Y. Kim, M.-H. Lee, Functions achieved by the hyaluronic acid derivatives coating and hydroxide film on bio-absorbed Mg, Appl. Surf. Sci. 473 (2019) 31–39.
[191] E. Khor, L.Y. Lim, Implantable applications of chitin and chitosan, Biomaterials 24 (13) (2003) 2339–2349.
[192] S. Fooladi, S.R. Kiahosseini, Creation and investigation of chitin/HA double-layer coatings on AZ91 magnesium alloy by dipping method, J. Mater. Res. 32 (13) (2017) 2532–2541.

[193] X. Liu, Z. Yue, T. Romeo, J. Weber, T. Scheuermann, S. Moulton, G. Wallace, Biofunctionalized anti-corrosive silane coatings for magnesium alloys, Acta Biomater. 9 (10) (2013) 8671–8677.
[194] Y. Pei, G. Zhang, C. Zhang, J. Wang, R. Hang, X. Yao, X. Zhang, Corrosion resistance, anticoagulant and antibacterial properties of surface-functionalized magnesium alloys, Mater. Lett. 234 (2019) 323–326.
[195] D. Mushahary, C. Wen, J.M. Kumar, J. Lin, N. Harishankar, P. Hodgson, G. Pande, Y. Li, Collagen type-I leads to in vivo matrix mineralization and secondary stabilization of Mg–Zr–Ca alloy implants, Colloids Surf. B Biointerfaces 122 (2014) 719–728.
[196] C. Liu, Y. Xin, X. Tian, P.K. Chu, Degradation susceptibility of surgical magnesium alloy in artificial biological fluid containing albumin, J. Mater. Res. 22 (7) (2007) 1806–1814.
[197] W.Y. Chan, K.S. Chian, M.J. Tan, In vitro metal ion release and biocompatibility of amorphous Mg67Zn28Ca5 alloy with/without gelatin coating, Mater. Sci. Eng. C 33 (8) (2013) 5019–5027.
[198] X. Xu, P. Lu, M. Guo, M. Fang, Cross-linked gelatin/nanoparticles composite coating on micro-arc oxidation film for corrosion and drug release, Appl. Surf. Sci. 256 (8) (2010) 2367–2371.
[199] C. Vepari, D.L. Kaplan, Silk as a biomaterial, Prog. Polym. Sci. 32 (8–9) (2007) 991–1007.
[200] P. Xiong, J. Yan, P. Wang, Z. Jia, W. Zhou, W. Yuan, Y. Li, Y. Liu, Y. Cheng, D. Chen, A pH-sensitive self-healing coating for biodegradable magnesium implants, Acta Biomater. 98 (2019) 160–173.
[201] W. Xu, K. Yagoshi, T. Asakura, M. Sasaki, T. Niidome, Silk fibroin as a coating polymer for sirolimus-eluting magnesium alloy stents, ACS Appl. Bio Mater. 3 (1) (2019) 531–538.
[202] C. Zhang, Z. Zhou, X. Wang, J. Liu, J. Sun, L. Wang, W. Ye, C. Pan, A multifunctional coating with silk fibroin/chitosan quaternary ammonium salt/heparin sodium for AZ31B magnesium alloy, Mater. Today Commun. 34 (2023) 105070.
[203] R. Zhang, S. Cai, G. Xu, H. Zhao, Y. Li, X. Wang, K. Huang, M. Ren, X. Wu, Crack self-healing of phytic acid conversion coating on AZ31 magnesium alloy by heat treatment and the corrosion resistance, Appl. Surf. Sci. 313 (2014) 896–904.
[204] X. Cui, Y. Li, Q. Li, G. Jin, M. Ding, F. Wang, Influence of phytic acid concentration on performance of phytic acid conversion coatings on the AZ91D magnesium alloy, Mater. Chem. Phys. 111 (2–3) (2008) 503–507.
[205] S. Yang, R. Sun, K. Chen, Self-healing performance and corrosion resistance of phytic acid/cerium composite coating on microarc-oxidized magnesium alloy, Chem. Eng. J. 428 (2022) 131198.
[206] W. Ng, M. Wong, F. Cheng, Stearic acid coating on magnesium for enhancing corrosion resistance in Hanks' solution, Surf. Coating. Technol. 204 (11) (2010) 1823–1830.
[207] J. Zhu, X. Dai, J. Xiong, Study on the preparation and corrosion resistance of hydroxyapatite/stearic acid superhydrophobic composite coating on magnesium alloy surface, AIP Adv. 9 (4) (2019).
[208] Y. Zhang, J. Xu, Y.C. Ruan, M.K. Yu, M. O'Laughlin, H. Wise, D. Chen, L. Tian, D. Shi, J. Wang, Implant-derived magnesium induces local neuronal production of CGRP to improve bone-fracture healing in rats, Nat. Med. 22 (10) (2016) 1160–1169.
[209] L. Tian, Y. Sheng, L. Huang, D.H.-K. Chow, W.H. Chau, N. Tang, T. Ngai, C. Wu, J. Lu, L. Qin, An innovative Mg/Ti hybrid fixation system developed for fracture fixation and healing enhancement at load-bearing skeletal site, Biomaterials 180 (2018) 173–183.
[210] N. Zheng, J. Xu, C.R. Ye, L. Chang, X. Wang, H. Yao, J. Wang, R. Zhang, Q. Xue, N. Tang, Magnesium Facilitates the Healing of Atypical Femoral Fractures: A Single-Cell Transcriptomic Study, 2022.
[211] J. Wang, J. Xu, X. Wang, L. Sheng, L. Zheng, B. Song, G. Wu, R. Zhang, H. Yao, N. Zheng, M.T. Yun Ong, P.S. Yung, L. Qin, Magnesium-pretreated periosteum for promoting bone-tendon healing after anterior cruciate ligament reconstruction, Biomaterials 268 (2021) 120576.
[212] S. Yoshizawa, A. Brown, A. Barchowsky, C. Sfeir, Magnesium ion stimulation of bone marrow stromal cells enhances osteogenic activity, simulating the effect of magnesium alloy degradation, Acta Biomater. 10 (6) (2014) 2834–2842.
[213] H.S. Han, I. Jun, H.K. Seok, K.S. Lee, K. Lee, F. Witte, D. Mantovani, Y.C. Kim, S. Glyn-Jones, J.R. Edwards, Biodegradable magnesium alloys promote angio-osteogenesis to enhance bone repair, Adv. Sci. 7 (15) (2020) 2000800.
[214] J.A. Maier, D. Bernardini, Y. Rayssiguier, A. Mazur, High concentrations of magnesium modulate vascular endothelial cell behaviour in vitro, Biochim. Biophys. Acta (BBA) - Mol. Basis Dis. 1689 (1) (2004) 6–12.
[215] D. Bernardini, A. Nasulewicz, A. Mazur, J. Maier, Magnesium and microvascular endothelial cells: a role in inflammation and angiogenesis, Front. Biosci. 10 (1–3) (2005) 1177–1182.
[216] Z. Zhai, X. Qu, H. Li, K. Yang, P. Wan, L. Tan, Z. Ouyang, X. Liu, B. Tian, F. Xiao, The effect of metallic magnesium degradation products on osteoclast-induced osteolysis and attenuation of NF-κB and NFATc1 signaling, Biomaterials 35 (24) (2014) 6299–6310.
[217] H. Xie, Z. Cui, L. Wang, Z. Xia, Y. Hu, L. Xian, C. Li, L. Xie, J. Crane, M. Wan, PDGF-BB secreted by preosteoclasts induces angiogenesis during coupling with osteogenesis, Nat. Med. 20 (11) (2014) 1270–1278.
[218] M. Hamushan, W. Cai, Y. Zhang, Z. Ren, J. Du, S. Zhang, C. Zhao, P. Cheng, X. Zhang, H. Shen, High-purity magnesium pin enhances bone consolidation in distraction osteogenesis via regulating Ptch protein activating Hedgehog-alternative Wnt signaling, Bioact. Mater. 6 (6) (2021) 1563–1574.
[219] J. Wang, J. Xu, B. Song, D.H. Chow, P.S.-H. Yung, L. Qin, Magnesium (Mg) based interference screws developed for promoting tendon graft incorporation in bone tunnel in rabbits, Acta Biomater. 63 (2017) 393–410.
[220] P. Cheng, P. Han, C. Zhao, S. Zhang, H. Wu, J. Ni, P. Hou, Y. Zhang, J. Liu, H. Xu, High-purity magnesium interference screws promote fibrocartilaginous entheses regeneration in the anterior cruciate ligament reconstruction rabbit model via accumulation of BMP-2 and VEGF, Biomaterials 81 (2016) 14–26.
[221] C.-C. Hung, A. Chaya, K. Liu, K. Verdelis, C. Sfeir, The role of magnesium ions in bone regeneration involves the canonical Wnt signaling pathway, Acta Biomater. 98 (2019) 246–255.
[222] J. Zhang, X. Ma, D. Lin, H. Shi, Y. Yuan, W. Tang, H. Zhou, H. Guo, J. Qian, C. Liu, Magnesium modification of a calcium phosphate cement alters bone marrow stromal cell behavior via an integrin-mediated mechanism, Biomaterials 53 (2015) 251–264.
[223] L.-Z. Zheng, J.-L. Wang, J.-K. Xu, X.-T. Zhang, B.-Y. Liu, L. Huang, R. Zhang, H.-Y. Zu, X. He, J. Mi, Magnesium and vitamin C supplementation attenuates steroid-associated osteonecrosis in a rat model, Biomaterials 238 (2020) 119828.
[224] B. Dai, X. Li, J. Xu, Y. Zhu, L. Huang, W. Tong, H. Yao, D.H.-k. Chow, L. Qin, Synergistic effects of magnesium ions and simvastatin on attenuation of high-fat diet-induced bone loss, Bioact. Mater. 6 (8) (2021) 2511–2522.
[225] P. Han, P. Cheng, S. Zhang, C. Zhao, J. Ni, Y. Zhang, W. Zhong, P. Hou, X. Zhang, Y. Zheng, Y. Chai, In vitro and in vivo studies on the degradation of high-purity Mg (99.99wt.%) screw with femoral intracondylar fractured rabbit model, Biomaterials 64 (2015) 57–69.
[226] A. Chaya, S. Yoshizawa, K. Verdelis, N. Myers, B.J. Costello, D.T. Chou, S. Pal, S. Maiti, P.N. Kumta, C. Sfeir, In vivo study of magnesium plate and screw degradation and bone fracture healing, Acta Biomater. 18 (2015) 262–269.
[227] K. Jähn, H. Saito, H. Taipaleenmäki, A. Gasser, N. Hort, F. Feyerabend, H. Schlüter, J.M. Rueger, W. Lehmann, R. Willumeit-Römer, E. Hesse, Intramedullary Mg2Ag nails augment callus formation during fracture healing in mice, Acta Biomater. 36 (2016) 350–360.
[228] P. Cheng, P. Han, C. Zhao, S. Zhang, X. Zhang, Y. Chai, Magnesium inference screw supports early graft incorporation with inhibition of graft degradation in anterior cruciate ligament reconstruction, Sci. Rep. 6 (2016) 26434.
[229] J. Wang, J. Xu, W. Fu, W. Cheng, K. Chan, P.S.-h. Yung, L. Qin, Biodegradable magnesium screws accelerate fibrous tissue mineralization at the tendon-bone insertion in anterior cruciate ligament reconstruction model of rabbit, Sci. Rep. 7 (2017) 40369.
[230] K.F. Farraro, N. Sasaki, S.L. Woo, K.E. Kim, M.M. Tei, A. Speziali, P.J. McMahon, Magnesium ring device to restore function of a transected anterior cruciate ligament in the goat stifle joint, J. Orthop. Res. : official publication of the Orthopaedic Research Society 34 (11) (2016) 2001–2008.
[231] B. Zhang, W. Zhang, F. Zhang, C. Ning, M. An, K. Yang, L. Tan, Q. Zhang, Degradable magnesium alloy suture promotes fibrocartilaginous interface regeneration in a rat rotator cuff transosseous repair model, J. Magnesium Alloys (2022).
[232] Z.Z. Zhang, Y.F. Zhou, W.P. Li, C. Jiang, Z. Chen, H. Luo, B. Song, Local administration of magnesium promotes meniscal healing through homing of endogenous stem cells: a proof-of-concept study, Am. J. Sports Med. 47 (4) (2019) 954–967.
[233] Y. Chen, Y. Sun, X. Wu, J. Lou, X. Zhang, Z. Peng, Rotator cuff repair with biodegradable high-purity magnesium suture anchor in sheep model, Journal of Orthopaedic Translation 35 (2022) 62–71.
[234] M. Hamushan, W. Cai, Y. Zhang, Z. Ren, J. Du, S. Zhang, C. Zhao, P. Cheng, X. Zhang, H. Shen, High-purity magnesium pin enhances bone consolidation in distraction osteogenesis via regulating Ptch protein activating Hedgehog-alternative Wnt signaling, Bioact. Mater. 6 (6) (2021) 12.
[235] M. Hamushan, W. Cai, Y. Zhang, T. Lou, S. Zhang, X. Zhang, P. Cheng, C. Zhao, P. Han, High-purity magnesium pin enhances bone consolidation in distraction osteogenesis model through activation of the VHL/HIF-1α/VEGF signaling, J. Biomater. Appl. 35 (2) (2020) 224–236.
[236] D. Zhao, S. Huang, F. Lu, B. Wang, L. Yang, L. Qin, K. Yang, Y. Li, W. Li, W. Wang, S. Tian, X. Zhang, W. Gao, Z. Wang, Y. Zhang, X. Xie, J. Wang, J. Li, Vascularized bone grafting fixed by biodegradable magnesium screw for treating osteonecrosis of the femoral head, Biomaterials 81 (2016) 84–92.
[237] J. Sun, Z. Li, S. Liu, T. Xia, J. Shen, Biodegradable magnesium screw, titanium screw and direct embedding fixation in pedicled vascularized iliac bone graft transfer for osteonecrosis of the femoral head: a randomized controlled study, J. Orthop. Surg. Res. 18 (1) (2023) 523.
[238] H. Windhagen, K. Radtke, A. Weizbauer, J. Diekmann, Y. Noll, U. Kreimeyer, R. Schavan, C. Stukenborg-Colsman, H. Waizy, Biodegradable magnesium-based screw clinically equivalent to titanium screw in hallux valgus surgery: short term results of the first prospective, randomized, controlled clinical pilot study, Biomed. Eng. Online 12 (2013) 62.
[239] K. Xie, L. Wang, Y. Guo, S. Zhao, Y. Yang, D. Dong, W. Ding, K. Dai, W. Gong, G. Yuan, Y. Hao, Effectiveness and safety of biodegradable Mg-Nd-Zn-Zr alloy screws for the treatment of medial malleolar fractures, J Orthop Translat 27 (2021) 96–100.
[240] J.N. Katz, Z.E. Zimmerman, H. Mass, M.C. Makhni, Diagnosis and management of lumbar spinal stenosis: a review, JAMA 327 (17) (2022) 1688–1699.
[241] A.K. Chan, V. Sharma, L.C. Robinson, P.V. Mummaneni, Summary of guidelines for the treatment of lumbar spondylolisthesis, Neurosurgery Clinics 30 (3) (2019) 353–364.
[242] R.C. Campbell, R.J. Mobbs, V.M. Lu, J. Xu, P.J. Rao, K. Phan, Posterolateral fusion versus interbody fusion for degenerative spondylolisthesis: systematic review and meta-analysis, Global Spine J. 7 (5) (2017) 482–490.

[243] D. Meng, Lumbar interbody fusion: recent advances in surgical techniques and bone healing strategies, Eur. Spine J.: official publication of the European Spine Society, the European Spinal Deformity Society, and the European Section of the Cervical Spine Research Society 30 (1) (2021).
[244] R. Verma, S. Virk, S. Qureshi, Interbody fusions in the lumbar spine: a review, HSS J. : the musculoskeletal journal of Hospital for Special Surgery 16 (2) (2020) 162–167.
[245] A. Cruz, A.E. Ropper, D.S. Xu, M. Bohl, E.M. Reece, S.J. Winocour, E. Buchanan, G. Kaung, Failure in lumbar spinal fusion and current management modalities, Semin. Plast. Surg. 35 (1) (2021) 54–62.
[246] F. Veronesi, M. Sartori, C. Griffoni, M. Valacco, G. Tedesco, P.F. Davassi, A. Gasbarrini, M. Fini, G. Barbanti Brodano, Complications in spinal fusion surgery: a systematic review of clinically used cages, J. Clin. Med. 11 (21) (2022) 6279.
[247] Y. Chen, X. Wang, X. Lu, L. Yang, H. Yang, W. Yuan, D. Chen, Comparison of titanium and polyetheretherketone (PEEK) cages in the surgical treatment of multilevel cervical spondylotic myelopathy: a prospective, randomized, control study with over 7-year follow-up, Eur. Spine J. 22 (7) (2013) 1539–1546.
[248] C.V. Wrangel, A. Karakoyun, K.M. Buchholz, O. Süss, T. Kombos, J. Woitzik, P. Vajkoczy, M. Czabanka, Fusion rates of intervertebral polyetheretherketone and titanium cages without bone grafting in posterior interbody lumbar fusion surgery for degenerative lumbar instability, J. Neurol. Surg. Cent. Eur. Neurosurg. 78 (6) (2017) 556–560.
[249] S.A. Zadegan, A. Abedi, S.B. Jazayeri, H.N. Bonaki, A.R. Vaccaro, V. Rahimi-Movaghar, Clinical application of ceramics in anterior cervical discectomy and fusion: a review and update, Global Spine J. 7 (4) (2017) 343–349.
[250] Y. Assem, R.J. Mobbs, M.H. Pelletier, K. Phan, W.R. Walsh, Radiological and clinical outcomes of novel Ti/PEEK combined spinal fusion cages: a systematic review and preclinical evaluation, Eur. Spine J. : official publication of the European Spine Society, the European Spinal Deformity Society, and the European Section of the Cervical Spine Research Society 26 (3) (2017) 593–605.
[251] W. Singhatanadgige, A. Sukthuayat, T. Tanaviriyachai, J. Kongtharvonskul, T. Tanasansomboon, S.J. Kerr, W. Limthongkul, Risk factors for polyetheretherketone cage subsidence following minimally invasive transforaminal lumbar interbody fusion, Acta Neurochir. 163 (9) (2021) 2557–2565.
[252] A. Kienle, N. Graf, H.-J. Wilke, Does impaction of titanium-coated interbody fusion cages into the disc space cause wear debris or delamination? Spine J. 16 (2) (2016) 235–242.
[253] K. Høy, C. Bünger, B. Niederman, P. Helmig, E.S. Hansen, H. Li, T. Andersen, Transforaminal lumbar interbody fusion (TLIF) versus posterolateral instrumented fusion (PLF) in degenerative lumbar disorders: a randomized clinical trial with 2-year follow-up, Eur. Spine J. : official publication of the European Spine Society, the European Spinal Deformity Society, and the European Section of the Cervical Spine Research Society 22 (9) (2013) 2022–2029.
[254] E. Van de Kelft, J. Van Goethem, Trabecular metal spacers as standalone or with pedicle screw augmentation, in posterior lumbar interbody fusion: a prospective, randomized controlled trial, Eur. Spine J. : official publication of the European Spine Society, the European Spinal Deformity Society, and the European Section of the Cervical Spine Research Society 24 (11) (2015) 2597–2606.
[255] J. Lebhar, P. Kriegel, P. Chatellier, Y. Breton, M. Ropars, D. Huten, Tantalum implants for posterior lumbar interbody fusion: a safe method at medium-term follow-up? Orthopaedics & traumatology, surgery & research : OTSR 106 (2) (2020) 269–274.
[256] B.W. Burkhardt, Y. Bullinger, S.J. Mueller, J.M. Oertel, The surgical treatment of pyogenic spondylodiscitis using carbon-fiber–reinforced polyether ether Ketone implants: personal experience of a series of 81 consecutive patients, World Neurosurgery 151 (2021) e495–e506.
[257] J. Li, M.L. Dumonski, Q. Liu, A. Lipman, J. Hong, N. Yang, Z. Jin, Y. Ren, W. Limthongkul, J.T. Bessey, J. Thalgott, G. Gebauer, T.J. Albert, A.R. Vaccaro, A multicenter study to evaluate the safety and efficacy of a stand-alone anterior carbon I/F Cage for anterior lumbar interbody fusion: two-year results from a Food and Drug Administration investigational device exemption clinical trial, Spine 35 (26) (2010) E1564–E1570.
[258] M. Laubach, P. Kobbe, D.W. Hutmacher, Biodegradable interbody cages for lumbar spine fusion: current concepts and future directions, Biomaterials 288 (2022) 121699.
[259] Y. Liu, H. Wu, S. Bao, H. Huang, Z. Tang, H. Dong, J. Liu, S. Chen, N. Wang, Z. Wu, Z. Zhang, L. Shi, X. Li, Z. Guo, Clinical application of 3D-printed biodegradable lumbar interbody cage (polycaprolactone/β-tricalcium phosphate) for posterior lumbar interbody fusion, J. Biomed. Mater. Res. B Appl. Biomater. 111 (7) (2023) 1398–1406.
[260] N. Xu, F. Wei, X. Liu, L. Jiang, H. Cai, Z. Li, M. Yu, F. Wu, Z. Liu, Reconstruction of the upper cervical spine using a personalized 3D-printed vertebral body in an adolescent with ewing sarcoma, Spine 41 (1) (2016) E50–E54.
[261] R. Agarwal, A.J. García, Biomaterial strategies for engineering implants for enhanced osseointegration and bone repair, Adv. Drug Deliv. Rev. 94 (2015) 53–62.
[262] P. Xiu, Z. Jia, J. Lv, C. Yin, Y. Cheng, K. Zhang, C. Song, H. Leng, Y. Zheng, H. Cai, Z. Liu, Tailored surface treatment of 3D printed porous Ti6Al4V by microarc oxidation for enhanced osseointegration via optimized bone in-growth patterns and interlocked bone/implant interface, ACS Appl. Mater. Interfaces 8 (28) (2016) 17964–17975.
[263] Y. Zhang, P. Xiu, Z. Jia, T. Zhang, C. Yin, Y. Cheng, H. Cai, K. Zhang, C. Song, H. Leng, W. Yuan, Z. Liu, Effect of vanadium released from micro-arc oxidized porous Ti6Al4V on biocompatibility in orthopedic applications, Colloids Surf. B Biointerfaces 169 (2018) 366–374.
[264] R. Baron, M. Kneissel, WNT signaling in bone homeostasis and disease: from human mutations to treatments, Nat. Med. 19 (2) (2013) 179–192.
[265] J. Pierre Marie, Targeting integrins to promote bone formation and repair, Nat. Rev. Endocrinol. 9 (5) (2013) 288–295.
[266] D. Zou, L. Yue, Z. Fan, Y. Zhao, H. Leng, Z. Sun, W. Li, Biomechanical analysis of lumbar interbody fusion cages with various elastic moduli in osteoporotic and non-osteoporotic lumbar spine: a finite element analysis, Global Spine J. (2023) 21925682231166612.
[267] D. Zou, Z. Sun, S. Zhou, W. Zhong, W. Li, Hounsfield units value is a better predictor of pedicle screw loosening than the T-score of DXA in patients with lumbar degenerative diseases, Eur. Spine J. : official publication of the European Spine Society, the European Spinal Deformity Society, and the European Section of the Cervical Spine Research Society 29 (5) (2020) 1105–1111.
[268] L.-n. Wang, B. Yuan, F. Chen, B.-w. Hu, Y.-m. Song, X.-f. Li, Q. Zhou, X. Yang, X.-d. Zhu, H.-l. Yang, Ability of a novel biomimetic titanium alloy cage in avoiding subsidence and promoting fusion: a goat spine model study, Mater. Des. 213 (2022) 110361.
[269] F. Zhang, H. Xu, H. Wang, F. Geng, X. Ma, M. Shao, S. Xu, F. Lu, J. Jiang, Quantitative analysis of near-implant magnesium accumulation for a Si-containing coated AZ31 cage from a goat cervical spine fusion model, BMC Muscoskel. Disord. 19 (1) (2018) 105.
[270] D. Daentzer, E. Willbold, K. Kalla, I. Bartsch, W. Masalha, M. Hallbaum, C. Hurschler, T. Kauth, D. Kaltbeitzel, C. Hopmann, B. Welke, Bioabsorbable interbody magnesium-polymer cage: degradation kinetics, biomechanical stiffness, and histological findings from an ovine cervical spine fusion model, Spine 39 (20) (2014) E1220–E1227.
[271] X. Guo, H. Xu, F. Zhang, F. Lu, Bioabsorbable high-purity magnesium interbody cage: degradation, interbody fusion, and biocompatibility from a goat cervical spine model, Ann. Transl. Med. 8 (17) (2020) 1054.
[272] W. Qiao, K.H.M. Wong, J. Shen, W. Wang, J. Wu, J. Li, Z. Lin, Z. Chen, J. P. Matinlinna, Y. Zheng, S. Wu, X. Liu, K.P. Lai, Z. Chen, Y.W. Lam, K.M. C. Cheung, K.W.K. Yeung, TRPM7 kinase-mediated immunomodulation in macrophage plays a central role in magnesium ion-induced bone regeneration, Nat. Commun. 12 (1) (2021) 2885.
[273] M. Seelig, A study of magnesium wire as an absorbable suture and ligature material, Arch. Surg. 8 (2) (1924) 669–680.
[274] E.W. Andrews, Absorbable metal clips as substitutes for ligatures and deep sutures in wound closure, J. Am. Med. Assoc. 69 (4) (1917) 278–281.
[275] J.M. Seitz, D. Utermöhlen, E. Wulf, C. Klose, F.W. Bach, The manufacture of resorbable suture material from magnesium–drawing and stranding of thin wires, Adv. Eng. Mater. 13 (12) (2011) 1087–1095.
[276] J. Zong, Q. He, Y. Liu, M. Qiu, J. Wu, B. Hu, Advances in the development of biodegradable coronary stents: a translational perspective, Materials today, Bio 16 (2022) 100368.
[277] Yue Zhang, Jian Cao, Mengmeng Lu, Yi Shao, Kewei Jiang, Xiaodong Yang, Xiaoyu Xiong, Shan Wang, Chenglin Chu, Feng Xue, Yingjiang Ye, Jing Bai, A biodegradable magnesium surgical staple for colonic anastomosis: *In vitro* and *in vivo* evaluation, Bioact Mater 22 (2023) 225–238.
[278] T. Yoshida, T. Fukumoto, T. Urade, M. Kido, H. Toyama, S. Asari, T. Ajiki, N. Ikeo, T. Mukai, Y. Ku, Development of a new biodegradable operative clip made of a magnesium alloy: evaluation of its safety and tolerability for canine cholecystectomy, Surgery 161 (6) (2017) 1553–1560.
[279] T. Urade, T. Yoshida, N. Ikeo, K. Naka, M. Kido, H. Toyama, K. Ueno, M. Tanaka, T. Mukai, T. Fukumoto, Novel biodegradable magnesium alloy clips compared with titanium clips for hepatectomy in a rat model, BMC Surg. 19 (1) (2019) 130.
[280] J. Vennemeyer, T. Hopkins, M. Hershcovitch, K. Little, M. Hagen, D. Minteer, D. Hom, K. Marra, S. Pixley, Initial observations on using magnesium metal in peripheral nerve repair, J. Biomater. Appl. 29 (8) (2015) 1145–1154.
[281] Y. Okamura, N. Hinata, T. Hoshiba, T. Nakatsuji, N. Ikeo, J. Furukawa, K. Harada, Y. Nakano, T. Fukumoto, T. Mukai, Development of bioabsorbable zinc–magnesium alloy wire and validation of its application to urinary tract surgeries, World J. Urol. (2020) 1–8.
[282] Y.H. Chang, C.C. Tseng, C.Y. Chao, C.H. Chen, S.Y. Lin, J.K. Du, Mg-Zn-Ca alloys for hemostasis clips for vessel ligation: in vitro and in vivo studies of their degradation and response, Materials 13 (13) (2020).
[283] J. Xue, S. Singh, Y. Zhou, A. Perdomo-Pantoja, Y. Tian, N. Gupta, T.F. Witham, W. L. Grayson, T.P. Weihs, A biodegradable 3D woven magnesium-based scaffold for orthopedic implants, Biofabrication 14 (3) (2022).